Engineering Geology 323 (2023) 107199

Contents lists available at ScienceDirect

Engineering Geology

journal homepage: www.elsevier.com/locate/enggeo

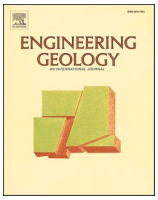

Rainfall infiltration and slope stability of alpine colluvial terraces subject to storms (NE Italy)

Paolo Paronuzzi, Alberto Bolla *

Dipartimento Politecnico di Ingegneria e Architettura, Università degli Studi di Udine, via Cotonificio 114, 33100 Udine, Italy

ARTICLE INFO

Keywords:
Rainfall-induced landslide
Infiltration modelling
Soil slip
Colluvial slope
Alpine terrace
Rainfall threshold

ABSTRACT

In the alpine environment, rainfall-induced shallow landslides can involve thin covers of colluvial soil (50–300 cm) on terraced belts that were formed as a result of fill-and-cut sedimentary processes that followed the deglaciation of the alpine valleys. Notably, research on shallow slope failures involving alpine terraces consisting of a near-flat upper ground surface ("tread") and a moderately steep scarp ("riser") is lacking in the literature. This paper describes the engineering geological characteristics and failure mechanisms of a large number of shallow landslides (soil slips or slide-debris flows) that were activated on alpine stratified colluvial terraces due to a rainstorm that hit the mountain area of the Friuli Venezia Giulia Region (NE Italy) on 21–22 June 1996. The paper reports data on the geomorphological and engineering geological characteristics of the soil slips acquired through extensive fieldwork and shows the outcomes of some two-dimensional seepage and slope stability analyses that were carried out in order to investigate the critical hydrological conditions and mechanisms that were responsible for the soil slip activation during and after rainfall. The soil slip activation can occur at two different stages during the infiltration process, based on the interacting water flows through the terrace tread and riser. The first critical stability condition is reached during the phases of greater precipitation intensity or at the end of the rainstorm because of the saturation of the top soil layer on the terrace riser and the subsequent formation of an ephemeral water table accompanied by a seepage sub-parallel to the slope face. The second critical condition is achieved some hours after the end of rainfall as a result of a tread-to-riser water outflow that is supplied by the water amount stored within the near-flat terrace tread during the peak rainfall stages (reservoir-like effect). This study also shows that a critical value of rainfall intensity of about 40–45 mm/h can cause the activation of soil slips in mountain basins characterised by a humid continental climate and by the occurrence of colluvial deposits with a high content of fine fraction. This critical value of rainfall intensity should be considered as a rainfall threshold for a basin-scale under geomorphological and geological conditions similar to those investigated in this paper.

1. Introduction

Shallow slope failures involving thin covers of colluvial soil (typically, thicknesses of 50–300 cm) are common hydrogeological instability processes in mountain areas that are hit by rainstorms. Although these shallow landslides are characterised by lower magnitude or volumes compared with rockslides, rockfalls and large earth mass movements, they can pose a severe threat to human settlements, in particular due to their multiple occurrences in relatively small areas during critical hydrological events (Stark and Hovius, 2001; Hungr et al., 2008; Froude and Petley, 2018; Bellugi et al., 2021). Rainfall-induced slope failures often evolve into debris flows (flow slides), causing damage to infrastructures and edifices and even casualties. In the last few decades, as a result of climate variations that are characterised by a general intensification of extreme meteorological events, these rainfall-induced landslides have occurred more and more frequently in various parts of the world, including the Italian Alpine territory (Gariano and Guzzetti, 2016; Haque et al., 2019).

In the literature, rainfall-induced shallow landslides were initially defined as "soil slips" with reference to numerous surficial slope failures that were identified in California (Kesseli, 1943; Rice et al., 1969; Campbell, 1974, 1975; Ellen and Fleming, 1987) and in some sectors of the Austrian Alps (Moser and Hohensinn, 1983) and the Italian Alps (Cancelli and Nova, 1985; Crosta, 1990, 1994; Montrasio, 2000). The

* Corresponding author.
E-mail address: alberto.bolla@uniud.it (A. Bolla).

https://doi.org/10.1016/j.enggeo.2023.107199
Received 30 January 2023; Received in revised form 26 May 2023; Accepted 31 May 2023
Available online 9 June 2023

term "disintegrating soil slips" was also used to highlight the peculiar evolution of these instability phenomena, which can be characterised by a fluidisation of the failed material, ultimately evolving as a downslope debris flow (Kesseli, 1943). More recently, the term "soil slip" has been used by various authors to describe rainfall-induced shallow slope failures that were recognised in other areas of California (Pike and Sobieszczyk, 2008), in Japan (Wakatsuki and Matsukura, 2008) and in the Italian Alps and Apennines (Crosta and Frattini, 2003; Guzzetti et al., 2004; D'Amato Avanzi et al., 2009; Montrasio et al., 2011; Gatto and Montrasio, 2023).

When considering the unified international classification system of landslide types that was first proposed by Varnes (1978) and subsequently modified by Cruden and Varnes (1996) and Hungr et al. (2014), a slope instability process characterised by an initial sliding of a soil mass (slump) and a subsequent fluidisation of the failed material can be classified as a complex landslide of the type slide-debris flow or slide-earth flow, depending on the specific grain size and plasticity of the involved materials. As a result, slide-debris (earth) flows were reported in studies that analysed shallow slope failures caused by rainstorms (Dai et al., 1999; Di Crescenzo and Santo, 2005; Wen and Aydin, 2005; Okada et al., 2007; Zhang et al., 2011).

The activation of a soil slip is driven by the rainfall infiltration process through the unsaturated–saturated colluvial cover, which first results in a decrease in the soil suction and then can determine an increase in pore-water pressure, nonetheless causing a reduction in the effective stress in the slope and, thus, a decrease in the shear strength along the potential failure surface (Johnson and Sitar, 1990; Ng and Shi, 1998; Gasmo et al., 2000; Godt et al., 2009; Rahardjo et al., 2010; Li et al., 2013; Kluger et al., 2020). A widely recognised failure mechanism of colluvial slopes is associated with the formation of a temporary sub-surface water table (Dapporto et al., 2005; Shakoor and Smithmyer, 2005; Sun et al., 2021). The possible occurrence of a sub-surface water table mainly depends on the permeability of the colluvial materials and the evolution of rainfall over time, in terms of both duration (D) and hourly intensity (I) (Segoni et al., 2018). However, the occurrence of shallow landslides was found to be strictly dependent on the regional characteristics related to both rainfall patterns and geological conditions of the soil slopes (D'Amato Avanzi et al., 2004; Giannecchini, 2006; Guzzetti et al., 2007, 2008; Cho, 2017; Salciarini et al., 2017). Therefore, proper analysis of the rainfall infiltration process must consider local situations to predict the stability condition of unsaturated soil slopes during and after the rainfall event.

Most reported cases of rainfall-induced landslides are related to shallow slope debris covers overlying a bedrock at constant depth, even assuming a stratified deposit made up of two, three or more soil layers with different hydrological properties (Crosta and Dal Negro, 2003; Dapporto et al., 2005; Cho, 2009; Ray et al., 2010; Jeong et al., 2017; Li et al., 2021). In several cases, the thickness of the soil cover is small compared with the total length of the slope and the failure surface is typically assumed as being parallel to the slope surface. Under these assumptions, the effect of rainfall infiltration on the pore pressure distribution is commonly investigated assuming a one-dimensional infiltration model and the related stability condition of the slope is analysed according to the simple infinite slope approach (Dapporto et al., 2005; Shakoor and Smithmyer, 2005; Baum et al., 2010; Ray et al., 2010; Li et al., 2013; Cho, 2017; Damiano et al., 2017; Balzano et al., 2019).

Some studies have reported slope instability processes caused by rainstorms on man-made terraced slopes that were designed for agricultural purposes in cultivated mountainous areas of the Mediterranean region (Crosta et al., 2003; Camera et al., 2014; Cevasco et al., 2014; Schilirò et al., 2018). However, this artificial terraced landform is made up of a dry-stone retaining wall and a near-horizontal surface on a back-filled material. A number of studies have also focused on irrigation-induced landslides affecting very thick terraced deposits of loess, clays and gravels on the high plateaus of China and Peru (Hou et al., 2018; Peng et al., 2018; Graber et al., 2021).

In the alpine environment, thin deposits of colluvial soils also occur along terraced belts that were formed as a result of fill-and-cut sedimentary processes that followed the deglaciation of the alpine valleys. These colluvial deposits can be involved in slope instability processes when subject to rainstorms. Differently from the cases previously discussed, alpine terraces consist of a flat or gently dipping upper ground surface (the "tread") and a moderately steep scarp (the "riser"). This terraced geometry, caused by geological processes that occurred in the last 20,000 years, does not allow for an analysis approach that assumes the simple infinite slope scheme. In fact, the rainfall infiltration process and the related slope stability of the terrace depend on the mutual interaction between the tread and the riser. Remarkably, research on rainfall-induced shallow landslides involving natural alpine terraces is lacking in the literature. As a result, this paper represents the first attempt to investigate the rainfall infiltration process and the slope stability of alpine colluvial terraces subject to intense precipitation.

This work describes the engineering geological characteristics and failure mechanisms of multiple shallow landslides caused by a rainstorm that hit the mountain area of the Friuli Venezia Giulia (FVG) Region (NE Italy) on 21–22 June 1996 (Fig. 1). In particular, the paper illustrates the geomorphological and geotechnical characteristics of a large number of soil slips (slide-debris flows) that were activated on the alpine colluvial terraces of the Chiarsò valley, in the surroundings of the village of Paularo (Fig. 2). The extensive fieldwork was accompanied by some two-dimensional seepage and slope stability analyses that were carried out in order to investigate the critical hydrological conditions and mechanisms that were responsible for the soil slip activation during and after rainfall.

2. Case study: The rainstorm on 21–22 June 1996 in the Chiarsò valley

2.1. Rainfall data

The northern mountain area of FVG (Carnic Alps) is characterised by a humid continental climate (Dfb of the Köppen-Geiger climate classification; Beck et al., 2018), with average monthly temperatures between 4.4 °C and 14.8 °C. Due to the proximity of the northern Adriatic Sea (Fig. 1), FVG is typically subject to the direct influx of sirocco winds blowing from the sea that are rich in humidity. The humid air masses reach the first reliefs after having crossed the plain and, as they rise and cool down, they condense giving rise to intense rainfall. In the Carnic Alps area, the dominant winds are frequently channelled into the valleys, modifying the air circulation and resulting in possible situations of stagnation, which are often associated with very strong storms. The average yearly rainfall (AYR) for the study area, calculated in the period 1923–2017 (gauge station of Paularo), is equal to 1719 mm, with a seasonal distribution that shows two peaks of average monthly precipitation: a first peak in November (197.7 mm) and a second one in June (177.1 mm).

Previous studies on heavy rainfall that affected mountain basins of the Carnic Alps demonstrated that the critical hydrological conditions were reached for threshold values associated with a cumulative rainfall height of 150 mm in 24 h (Paronuzzi and Vanon, 1995; Paronuzzi et al., 1998). In several cases within the study area, 24-h rainfall height peaks exceeded both the mean value of 123 mm of the maximum yearly value (MYV) for a 24-h rain duration and the 10% of AYR (172 mm) (Fig. 3a). The 24-h rainfall on 22 June 1996 (295.8 mm) is the second highest peak ever recorded in the study area, which is very close to the maximum value of 24-h rainfall registered at Paularo on 11 September 1983 (300 mm) (Fig. 3a).

When considering the main critical hydrologic events that have occurred in the Alpine area of FVG in the last 35 years, the most significant slope instability events occurred in concomitance with rainfall of high intensity ($40\ mm/h \leq I \leq 100\ mm/h$) and low duration ($D = 1–6$ h) (Fig. 3b). These situations correspond to hydrologic events that, in the

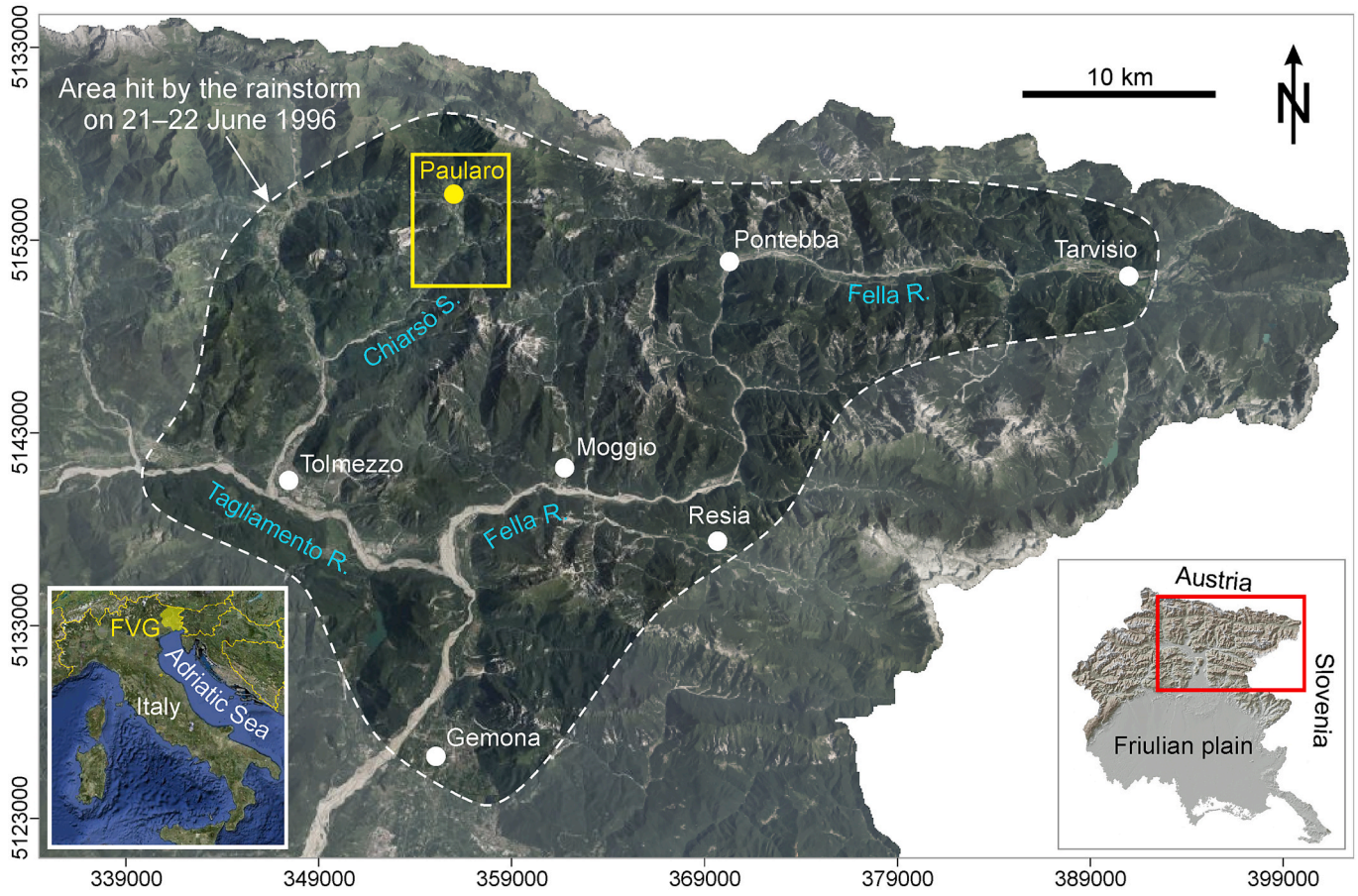

Fig. 1. The mountain area of the Friuli Venezia Giulia Region (NE Italy) that was hit by the rainstorm on 21–22 June 1996. Coordinates are in the local RDN2008/TM33NE system.

FVG area, have a return period (Tr) variable from 5 to 10 years (40–45 mm/h, over a 1 h rainfall) to 50–200 years for the most severe circumstances (90 mm/h for 1 h, and 50 mm/h for 3 h) (Fig. 3b). The return period, estimated through various Gumbel methods, actually varies according to the specific Alpine sector considered. However, the values of Tr reported here are only indicative to highlight the remarkable recurrence of intense precipitation events.

During critical hydrologic events occurring in the Carnic Alps, rainfall is commonly characterised by a considerable hourly intensity, with maximum values that often exceed 40 mm/h and can even reach values of 90–100 mm/h. In these circumstances, many surficial slope failures can occur, which tend to be concentrated in rather small areas characterised by the maximum values of rainfall intensity. In this regard, the rainstorm that hit the mountain area of Carnia in FVG on 11 September 1983 was emblematic, causing about 400 shallow landslides in a restricted area between the villages of Paularo (Chiarsò valley) and Paluzza (Bût valley). This extreme meteorological event occurred in a very short period, between 00:00 A.M. and 06:00 A.M. (GMT + 1) on 11 September 1983, and was characterised by a cumulated rainfall height of 270 mm, with a maximum hourly intensity estimated at 60 mm/h (Querini, 1984).

Analogously, the rainstorm that hit a large mountain area of FVG on 21 and 22 June 1996 caused dozens of soil slips, most of which were activated on the alpine terraces and colluvial slopes along the Chiarsò valley in the nearby of Paularo, including the hamlets of Dierico, Dioor and Salino (Fig. 2). From a meteorological point of view, this extreme meteorological event was the tail of a larger Atlantic perturbation coming from the west, which had already hit northern Italy with disastrous consequences. The precipitation pattern has been reconstructed according to the rainfall data registered by a number of gauge stations that were located in the area affected by the storm event (Paronuzzi et al., 1998). The following highest values of cumulated rainfall were measured on 21–22 June 1996 (Fig. 4a): 504.8 mm at Pontebba, 485.4 mm at Moggio, 316.8 mm at Paularo, and 290.0 mm at Resia. At the same gauge stations, very high hourly intensity peaks were recorded, ranging from 74 mm/h at Pontebba to 90 mm/h at Paularo (Fig. 4b) and 100 mm/h at Moggio, which is the maximum intensity value that was recorded during the storm event.

The combined analysis of precipitation data and temporal occurrence of hydrogeological instabilities allowed for the identification of a critical value of hourly intensity of about 40–45 mm/h that was responsible for the activation of the soil slips in the mountain basins that were hit by the rainstorm. In the Chiarsò valley, most of the slide-debris flows took place in the morning of 22 June, around 10:00 A.M., according to the numerous eyewitnesses. When analysing the pattern of hourly precipitation that was recorded at the Paularo gauge station (Fig. 4b), an intensity value equal to 90 mm/h was recorded at 10:00 A.M., which is the maximum rainfall intensity that characterised the rainstorm on 21–22 June 1996 in the Chiarsò valley. The considerable concentration of shallow landslides in a small area, such as that of the terraced slopes of Dierico and Dioor, reflects the limited extension and the stationing of cells of intense precipitation that were formed during the storm. Remarkably, numerous eyewitnesses related the occurrence of abrupt variations in the rainfall intensity within short distances between adjacent areas.

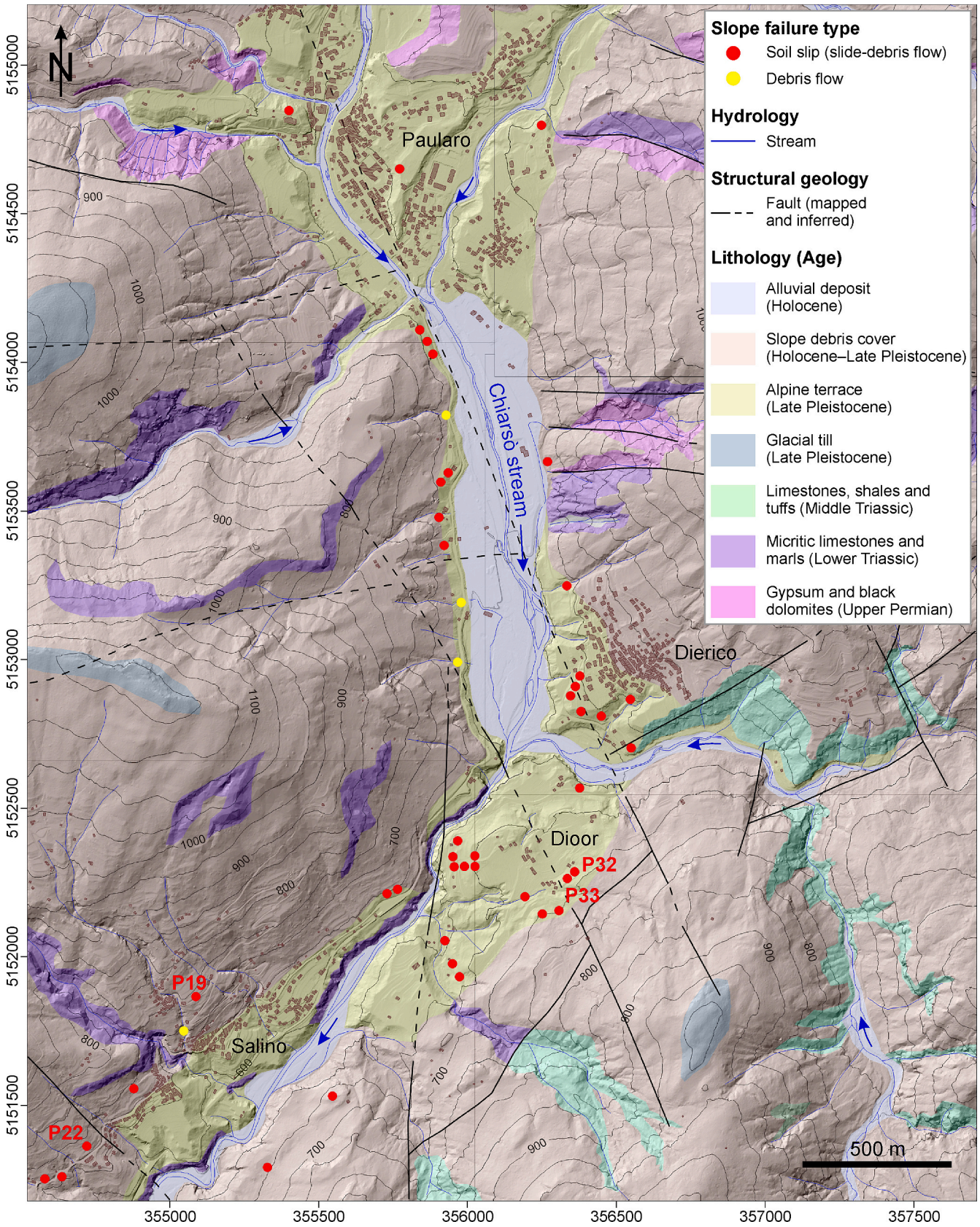

Fig. 2. Lithological map of the Chiarsò valley showing the location of the shallow landslides that occurred on 22 June 1996. The codes of the soil slips shown in Figs. 6 and 7 are reported. Coordinates are in the local RDN2008/TM33NE system.

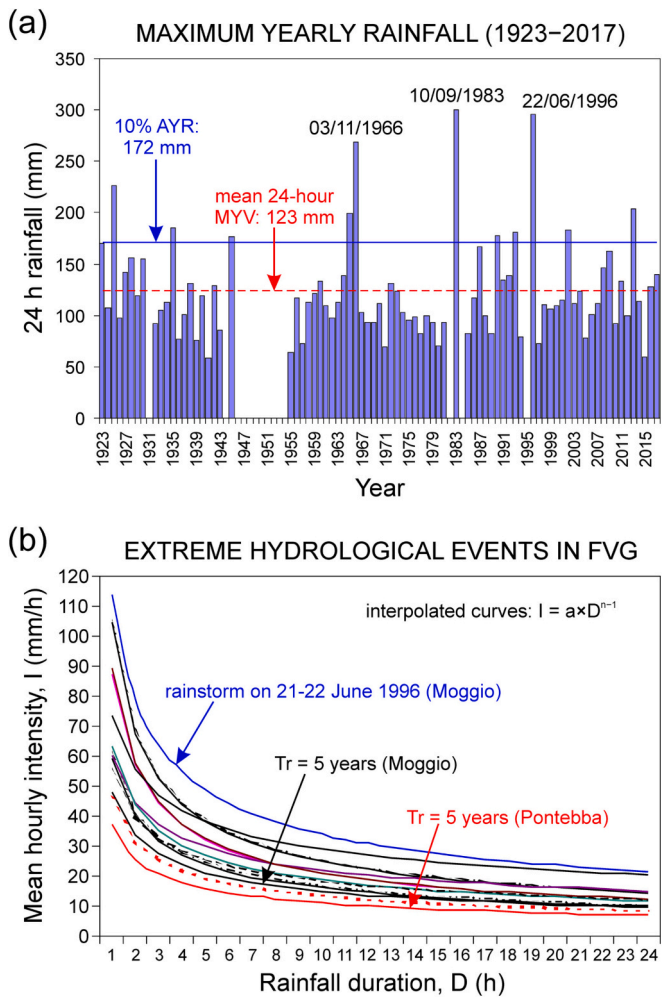

Fig. 3. (a) Maximum yearly values of 24-h rainfall recorded at the gauge station of Paularo (Chiarsò valley) over the period 1923–2017. (b) Critical rainfall curves calculated on the basis of historical extreme hydrological events that caused shallow landslides in the mountain basins of FVG during the period 1923–2017.

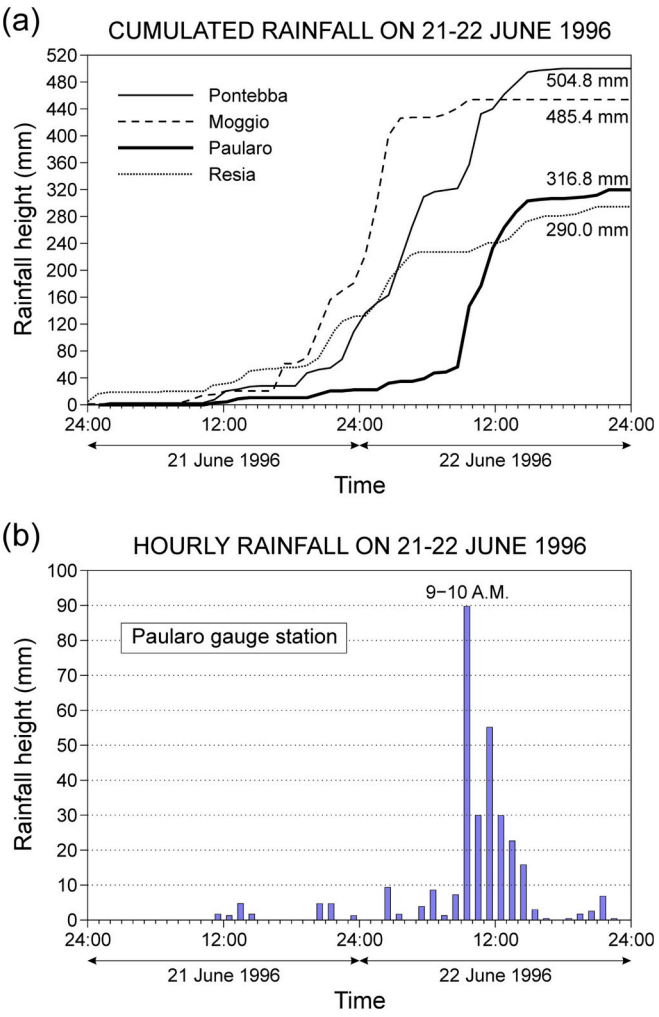

Fig. 4. (a) Cumulative rainfall measured by some gauge stations located in the mountain area of FVG hit by the rainstorm on 21–22 June 1996 (for their location, see Fig. 1). (b) Hourly rainfall intensity (mm/h) recorded by the gauge station of Paularo on 21–22 June 1996.

2.2. The alpine terraced system

One of the most significant alpine landscape features is the occurrence and wide distribution of terraced belts characterised by distinct elevations and heights above the valley floor (thalweg). The single terrace is made up of two geomorphological units: (i) the flat or low-inclined tread and (ii) the adjacent riser. During the Last Glacial Maximum (LGM), the Alpine troughs were occupied by large valley glaciers, and the maximum extension of the ice volume occurred between 26 and 23 ka cal. BP (Seguinot et al., 2018). Terracing of the alpine valleys is the consequence of repeated fill-and-cut sedimentary processes that characterised the end of the Late Pleistocene in the Alps, especially during the Alpine Lateglacial (about 18.9–11.7 ka cal. BP, Ivy-Ochs et al., 2023), i.e. the phase that started after the rapid retreat of the valley glaciers that occurred at about 19–18 ka cal. BP. The deglaciation of the alpine valleys was followed by repeated erosive and depositional events that were responsible for the formation of the typical alpine terrace sequences (Surian, 1996; Surian and Pellegrini, 2000).

Current morphological-stratigraphical data indicates that alpine terraces mainly formed during a restricted time interval, essentially between 18 and 12 ka cal. BP (Ivy-Ochs et al., 2023). Alpine terracing includes both the typical alluvial belts flanking the main river course and the terraced strips that are cut into the lateral fans deposited by the secondary alluvial tributaries, especially when the fluvial catchments do not have a negligible size (Colucci et al., 2014). All these terraces have a geological origin and are extremely different from man-made terraced structures designed for cultivation purposes. The alpine terraces, in most cases covered by grass, represent the most important sectors of Alpine valleys used by local inhabitants for haymaking and herd pasture.

The Chiarsò valley is placed within the central sector of the Carnic Alps and is crossed by the homonymous stream. Its thalweg develops between elevations 520–860 m a.s.l., while the surrounding mountain peaks reach a maximum elevation of about 2200 m a.s.l. The main tributaries of the Chiarsò stream are the Ruat, Minischitte, Turriea and Muêia torrents, and the major villages are located on the terraces formed on their alluvial fans. The valley slopes are made up of an Upper Permian–Middle Triassic sequence consisting of (Fig. 2) (Venturini, 2001): (i) gypsum and black dolomites of the Bellerophon Formation (Fm.); (ii) dolomitic limestones, silty marls, sandstones and purplish siltstones belonging to the Werfen Fm.; and (iii) tuffaceous sandstones, shales and marly limestones of the Buchenstein Fm. Various deposits belonging to the Quaternary occur along the valley sides and the thalweg. The oldest Quaternary sediments are represented by isolated breccias and conglomeratic deposits of unknown age (Middle Pleistocene?), which are located along the lower slopes of the Chiarsò valley. Lateglacial terraces and Holocene alluvial deposits are also present along the valley, where numerous alluvial fans were deposited as a result of stream

erosive processes occurring during extreme rainfall events (Fig. 2).

According to findings of the geomorphological survey that was performed within this research, alpine terraces of the Chiarsò valley can be grouped into various terrace "orders", based on their elevation. The multi-order terrace system is evident at Paularo, on the alluvial fans created by the Turriea stream at the confluence with the Chiarsò river, and further downstream near Dierico and Dioor, at the confluence of the Muêia stream and the Chiarsò river (Figs. 2 and 5a). Fluvial terraces that were formed by the main course of the Chiarsò stream are made up of typical alluvial deposits, such as sandy gravels and gravelly sands, including several well-rounded cobbles and pebbles. These terraced fluvial deposits are some meters above the current active stream and characterise the lower order (T1) (Fig. 5b). Conversely, colluvial deposits with abundant silty matrix are distinctive of higher terrace orders (T2–T5) and are the typical geomorphological feature of the lateral fans deposited by the fluvial tributaries (Fig. 5b). In this second case, the wide spectrum of the grain size classes characterising the surface sediments (from blocks to silty loam), in most cases depends on the lithology of the rock masses outcropping in the alpine basin and along the upper steeper rock faces.

The occurrence of many sedimentary rock masses including widespread layers of marl and shale, together with the limited transport, favoured the formation of poorly selected sediments with a significant percentage of fines, especially silt. These poorly sorted sediments, which have a mixture of sandy gravel supported by a clayey silt matrix, characterise the colluvial terraces (T2–T5) that will be described in this work and that were involved in most of the shallow slope failures triggered by the 1996 rainstorm. Colluvial sediments and the related terraces are the consequence of the limited transport of soils, and denote the vicinity of a parent material or source rock mass that is rich in silt and clay minerals. Another characteristic of the colluvial terraces is the modest thickness of the surface sediment cover, which in most cases does not exceed 3 m and overlies at depth the weathered bedrock. This situation originates a strong permeability threshold at shallow depth and is decisive in influencing the local hydrogeological behaviour of both the tread and the adjacent scarp.

From the palaeo-environmental viewpoint, colluvial sediments were formed during a climatic situation that was cooler than the current one, reflecting the rapid climate modification that occurred during Pleistocene Lateglacial deglaciation, which caused diffuse snow and ice melting and the disappearance of the alpine permafrost cover. These climatic conditions caused the surface instability of the alpine slopes and the deposition of colluvial materials forming terraces with a shallow cover of silty matrix-supported sediments. Some thousands of years after their formation, the risers of the colluvial terraces have been subjected to some critical circumstances due to instability processes caused by heavy rainfall events that occurred during Holocene times. Storms characterised by critical precipitations, for both intensity and duration, caused localised failures and remobilised the colluvial materials forming the upper tread. Consequently, the tread edges shifted upslope and the failed sediments accumulated at the scarp toe.

These slope instability processes originated a new stratigraphy at the face of the terrace scarp, and the original in-situ colluvial sediments experienced a transportation process and a remobilisation that caused some modification in the original stratigraphical sequence and in the sedimentary texture. Newly formed landslide deposits covered the toe of the scarp thus increasing the sediment thickness at the base of the terrace, whereas the terrace crown moved upslope and exposed the in situ colluvial sequence. The repetition of slope instabilities and soil slips provoked the modification of slope angles along with stratigraphic changes. The soil slips that occurred on 22 June 1996 in the Chiarsò valley represent only one case, even if well documented, of the numerous and repeated critical rainfall events capable of triggering failure of colluvial terrace scarps. For this reason, the stratigraphy of the terrace riser, especially the middle and the lower part, is not the same as the upper terrace tread, and this difference has to be considered when designing the geological schematisation of the slope for modelling purposes.

The field survey performed immediately after the catastrophic rainstorm that occurred on 21–22 June 1996 allowed for the acquisition of fundamental data on the stratigraphy of colluvial terraces, both at the tread edges and along the scarps. The in-situ colluvial deposit forming the terrace tread is typically characterised by a three-layer stratigraphy:

(1) a surficial 20–40 cm-thick organic brown soil with roots and macro-voids;

(2) an intermediate 50–150 cm-thick olive-brown loamy colluvial layer; and

(3) a basal 30–150 cm-thick yellowish-brown clayey loamy colluvial layer mixed with abundant angular rock fragments derived from the local bedrock.

The weathered local bedrock is sometimes visible beneath the basal colluvial layer. The total thickness of the stratified colluvial deposit can vary according to the specific location and terrace order, but frequently ranges between 100 and 300 cm. Conversely, the terrace riser is commonly made up of a single and heterogeneous soil layer with roots and voids and a variable thickness that progressively increases from the tread border (20–40 cm) to the scarp toe (70–100 cm).

2.3. Soil slips occurrence

The rainstorm that hit the Chiarsò valley caused a large number of shallow landslides that occurred in a 4–5 km-long area of the valley, between the villages of Paularo and Salino (Fig. 2). This hydrogeological instability event resulted in extensive damage to infrastructures (road interruptions, retaining wall collapses), edifices (barn collapses, evacuation of threatened homes), farmlands (cultivation destruction) (Figs. 6 and 7), and also caused the death of one person run over by a debris flow. These shallow landslides can be referred to as soil slips (slide-debris flows) that involved colluvial deposits on both slope debris covers and alpine terraces (Figs. 2 and 5).

An extensive field campaign was performed immediately after the catastrophic event, in the period June–November 1996, and 52 landslides were recorded in this area. Each slope failure was localised on the regional technical map, coded (P1–P52), and surveyed to establish its geometric and geomorphological characteristics. The focus was on shallow failures involving the alpine terraced belts (Table 1), in order to investigate the geotechnical properties of the involved materials (Tables 2–4) and to analyse the infiltration process and stability condition of colluvial terraces.

During the field survey, the basic geological and geomorphological features of the shallow landslides were defined, including the geometry of the exposed failure scar, the stratigraphy of the colluvial deposit and the shape and extension of the slide mass. The analysis of the slide detachment surface as well as of the propagation of the failed material allowed us to recognise different evolutionary processes of the shallow landslides, starting from the initial sliding up to the final material deposition. When considering the geometry of the detachment surface, failure occurred through sliding in correspondence with a flat surface (planar sliding) or a slight circular surface (rotational sliding). Both situations were identified, even if the exact geometry of the failure surface was not always ascertained since the latter was only exposed in its upper part.

In a few cases, the slope instability process stopped immediately after the initial sliding and the mobilised material accumulated at a short distance at the toe of the landslide, resulting in a simple sliding (type A in Table 1). In most cases, after the initial sliding, the failure process was characterised by a fluidisation of the mobilised material and the slide mass lost its compactness, assuming the features of a debris flow that propagated downstream, often descending according to the maximum dip direction of the slope (Figs. 6 and 7). Two basic types of slide-debris

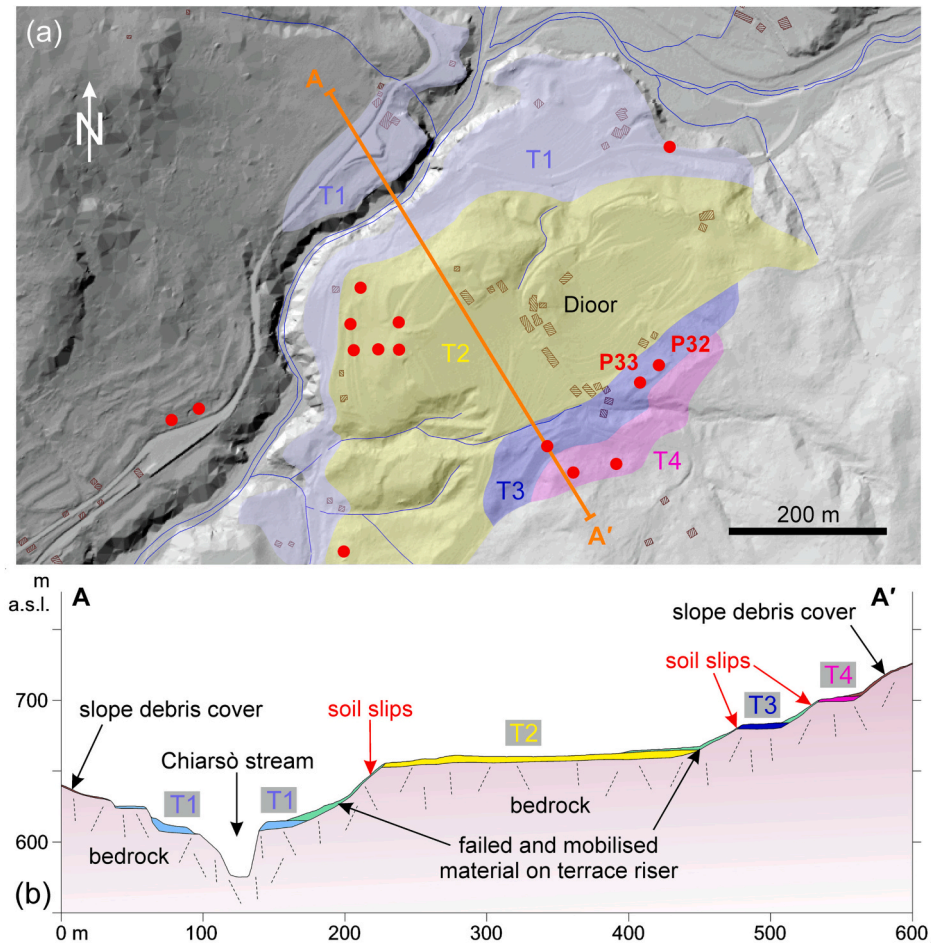

Fig. 5. (a) Map and (b) geological section of the alpine colluvial terraces at Dioor, showing the different terrace orders.

flow were distinguished: (i) a flow associated with a single transporting channel (type B in Table 1) Figs. 6a and 7; and (ii) a flow characterised by the formation of multiple transporting channels (type C in Table 1) (Fig. 6b). According to the data collected on the field, slope failure processes of the slide-debris flow type largely predominated (88%) over soil slips of the simple-sliding type (12%), thus demonstrating that the heavy rainfall characterising the storm on 21–22 June 1996 was high enough to cause, in most cases, the fluidisation of the colluvial materials that were involved in the slope failures.

The geometric data of the soil slips demonstrates the recurrent shallowness of the slope failures, the thickness (h) usually being included between 0.5 and 2.8 m, with an average value of 1.2 m (Table 1). The shape of the failure surfaces is commonly sub-rectangular (see for example slide P19 in Fig. 6a and slide P32 in Fig. 7), with a length (a) that is commonly larger than the width (b). The slide areas vary between a few tens of m^2 and a maximum of 600 m^2 (slide P43). The low depth and size of the failure surfaces determined small volumes of the mobilised material, which have been estimated from 10 m^3 to 480 m^3, with an average value of about 110 m^3 (Table 1).

The dip angle of the terrace risers involved in the shallow landslides essentially varies between 30° and 45°, with an average value close to 40° (Table 1). A dip angle higher than 45° was only ascertained for slide P45, which occurred on the uppermost terrace order of the valley, at the toe of steep rock scarps. The soil-slips involved alpine terraces occurring at various elevations above the valley floor (in most cases, in the range 600–700 m a.s.l.), which are characterised by different types of loose soil deposits. The failed slopes belong to various orders of alluvial terraces, which have been coded according to their elevation (T1–T5 in Tables 1 and 2nd Fig. 5), T5 being the highest terrace and T1 the lowest one, respectively. Most of the slope failures occurred on the lower terraces (T1–T3), with 14 soil slips that involved the intermediate terrace T2 (about 60% of the total), at elevations between 630 m a.s.l. and 660 m a.s.l. This concentration of side-debris flows mainly characterises the sub-unit T2b, where greater slope angles occur (43°).

The colluvial terraces were often cultivated or were kept as grass-covered areas for the collection of hay. In most cases, the presence of isolated trees or shrubs on the slopes prevented the occurrence of shallow instability processes, which only involved the grassy soil covers (Figs. 6 and 7). This fact demonstrates that, in these cases, the soil strength increase due to the development of the root systems (especially of trees) is large enough to inhibit the colluvial slope failure. This additional shear resistance contribution, which was also defined as root strength factor (RSF; Sidle et al., 1985), depends on the specific vegetation type and can reach effective cohesion values of 20–70 kPa, in most cases (Fan and Su, 2008; Zhang et al., 2010; Balzano et al., 2019).

The most frequent case of slope instability that has been observed on the field is the one related to soil slips that occurred at the top of the terrace risers, that is immediately below the edge of the terrace treads. In this case, the distance between the slide crown and the border of the tread (L) is lower than 2 m (Table 1). In some cases, multiple slide-debris flows affected the same scarp at several points that are located a few tens of meters away, but always immediately below the tread edge (Fig. 7). Some soil slips also occurred far from the upper border of the terrace scarp, i.e., in the middle or at the toe of the risers, with a distance from the tread border included in the range 5–15 m (Table 1).

Fig. 6. (a)–(b) Colluvial slopes near the village of Salino with distinct shallow slope failures associated with slide-debris flow. Note the highly disintegrated state of the failed material (for their location see Fig. 2).

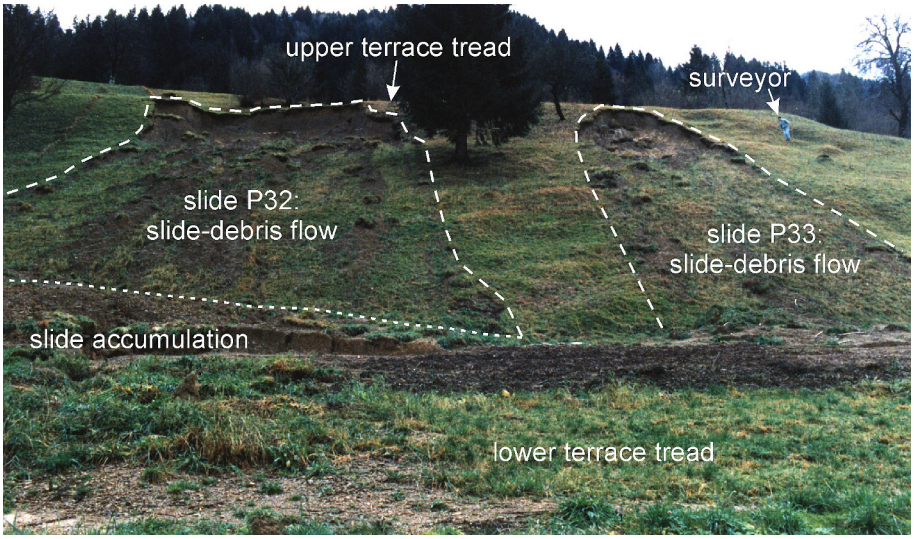

Fig. 7. Terraced slope near the hamlet of Dioor subjected to multiple soil slips of the slide-debris flow type (for their location see Fig. 2).

3. Geotechnical characterisation of colluvial materials

A number of soil samples were collected from 21 different shallow landslides that occurred along the Chiarsò valley on 21–22 June 1996, in order to investigate the geotechnical properties of the materials that were involved in the slope failures (Fig. 2). During the sampling procedure, particular attention was paid to avoid or reduce disturbance. The soil samples were collected from freshly exposed surfaces of the slides after cleaning the point of sampling by removing the surficial detritus. In most cases, the soil sampling was performed in correspondence with or immediately above the sliding surface of the soil slips. The soil samples were collected using steel cylindrical samplers with a cutting edge in order to minimise the contact and, thus, the side friction between the cutter walls and the coarser particles included in the soil mixture (cobbles and rock fragments). On the one hand, the increase in the volume of the sampler reduces the error associated with the

Table 1
Type and geometrical characteristics of the shallow landslides surveyed in the Chiarsò valley, ordered according to elevation and grouped according to various terrace orders.

Slide code	Type[a]	Location	Terrace order	Elevation	Length a	Width b	Thickness h	h/a	h/b	l[b]	Volume	Area	Terrace riser dip
				(m a.s.l.)	(m)	(m)	(m)	(–)	(–)	(m)	(m^3)	(m^2)	(°)
P45	B	Ravinis	T5	860	12.3	7.0	1.6	0.13	0.23	0.0	72	68	48
P34	B	Dioor	T4	735	15.2	5.2	1.4	0.09	0.27	8.2	58	62	34
P36	A	Dioor	T4	708	15.8	14.2	0.7	0.04	0.05	6.6	76	176	30
P32	B	Dioor	T3	690	18.4	17.8	2.8	0.15	0.16	0.0	480	257	40
P33	B	Dioor	T3	689	13.0	8.3	1.5	0.12	0.18	1.5	85	85	35
P35	B	Dioor	T3	680	9.5	18.3	1.4	0.15	0.08	0.0	127	137	40
				mean	14.0	11.8	1.6	0.11	0.16	2.7	150	131	38
P40	B	Dioor	T2b	658	14.1	13.1	2.1	0.15	0.16	6.0	203	145	44
P41	B	Dioor	T2b	658	8.0	5.0	1.0	0.13	0.20	5.0	21	31	44
P31	B	Dierico	T2b	647	12.2	9.7	1.0	0.08	0.10	12.0	62	93	44
P30	B	Dierico	T2b	645	11.8	7.8	0.9	0.08	0.12	0.0	43	72	39
P39	B	Dioor	T2b	645	8.2	5.8	1.3	0.16	0.22	–	32	37	45
P43	C	Dierico	T2b	645	23.0	33.2	1.0	0.05	0.04	1.2	400	600	43
P42	B	Dierico	T2b	640	15.0	6.2	1.3	0.09	0.21	2.0	63	73	42
P44	C	Dierico	T2b	640	27.2	9.8	0.8	0.03	0.08	14.0	112	209	41
P05	B	Paularo	T2b	640	31.5	20.0	0.7	0.02	0.04	15.0	231	495	44
P16	C	Plan di Laris	T2b	640	15.7	12.2	1.5	0.10	0.12	0.0	150	150	41
P37	A	Plan di Laris	T2b	635	14.5	6.1	1.0	0.07	0.17	12.0	46	69	45
				mean	16.5	11.7	1.1	0.09	0.13	6.7	124	179	43
P26	B	Dioor	T2a	630	8.6	4.6	0.5	0.06	0.11	9.0	10	31	31
P27	B	Dioor	T2a	630	10.8	12.6	1.5	0.14	0.12	–	107	107	30
P38	B	Dioor	T2a	630	14.0	8.7	1.2	0.09	0.14	–	77	96	33
				mean	11.1	8.6	1.1	0.10	0.12	9.0	65	78	31
P29	B	Dierico	T1	622	6.5	7.6	0.8	0.12	0.11	0.0	21	39	43
P28	A	Dierico	T1	620	8.0	6.3	0.6	0.08	0.10	1.0	16	40	43
P10	B	Paularo	T1	620	16.0	13.5	0.8	0.05	0.06	0.0	90	170	44
P13	B	Paularo	T1	615	13.0	10.5	1.5	0.12	0.14	–	107	107	35
				mean	10.9	9.5	0.9	0.09	0.10	0.3	59	89	41

[a] A: simple sliding; B: slide-debris flow with single transporting channel; C: slide-debris flow with multiple transporting channels.
[b] Distance between slide crown and terrace tread border.

Table 2
Grain size composition of the colluvial soils sampled from the shallow landslides in the Chiarsò valley.

Sample	Slide	Terrace order	Depth	Gravel	Sand	Silt	Clay
			(m)	(%)	(%)	(%)	(%)
P34S2	P34	T4	0.7	11.0	13.8	52.8	22.4
P36S2	P36	T4	0.5	0.0	42.5	41.0	16.6
P32S3	P32	T3	2.8	16.5	34.4	34.2	14.9
P33S2	P33	T3	1.3	34.7	21.2	31.3	12.7
P35S2	P35	T3	0.5	2.7	16.8	52.8	27.8
			mean	18.0	24.1	39.4	18.5
P30S2	P30	T2b	0.5	27.3	20.1	33.9	18.7
P39S2	P39	T2b	1.3	33.3	22.2	31.0	13.5
P43S3	P43	T2b	1.0	30.9	18.5	29.6	21.0
P42S3	P42	T2b	1.3	14.1	14.6	39.0	32.2
P05S2	P05	T2b	0.4	25.0	27.8	25.9	21.3
P37S4	P37	T2b	1.0	76.5	13.0	5.9	4.6
			mean	34.5	19.4	27.6	18.6
P26S4	P26	T2a	0.5	14.5	15.2	48.3	22.1
P27S2	P27	T2a	1.5	34.9	27.2	26.7	11.3
P38S2	P38	T2a	1.2	25.5	21.1	35.4	18.0
			mean	24.9	21.2	36.8	17.1
P29S3	P29	T1	0.8	0.7	77.9	18.2	3.2
P28S3	P28	T1	0.6	1.2	74.3	21.1	3.4
P10S3	P10	T1	0.8	29.5	18.2	36.4	16.0
P13S4	P13	T1	0.6	37.8	18.6	32.1	11.5
			mean	17.3	47.2	26.9	8.5

volumetric determination, but on the other hand, it increases the probability of contact with the coarser particles and, therefore, the extent of the disturbance. The objective difficulty of obtaining undisturbed samples from heterogeneous materials with a relevant coarse fraction, as commonly occurs in colluvial covers, must also be kept in mind. In these circumstances, a certain level of disturbance during the soil sampling must be considered unavoidable. The soil samples were then sealed and rapidly brought to the laboratory for the determination of their moisture properties.

The terraced deposits showed a variable grain size composition, in which the coarser fraction (gravel and sand) was in most cases equivalent to the finer fraction (silt and clay) (Fig. 8 and Table 2). The clay fraction was always lower than 35%, and often between 10 and 25%; whereas the silt/clay ratio remained quite constant and equal to 1.5. Remarkably, the grain size characteristics of the Late Pleistocene–Holocene deposits vary on the basis of the elevation and corresponding order of the terraces (Table 2), and three main groups of sediments are clearly recognisable in the diagram in Fig. 8, which shows the grain size distribution curves of the various samples analysed. The lowermost terrace T1 (610–630 m a.s.l.), which was formed during the Holocene, was characterised by the presence of fluvial sediments, sometimes well sorted as in the case of the silty sands of slides P28 and P29. These alluvial sediments showed a remarkable degree of grading, with values of the uniformity coefficient (Cu) equal to Cu = 4–7, and with a high sandy fraction (74–78%) accompanied by a certain content of silt (18–21%). The grain size distribution curves of these well graded silty sands are clearly differentiable (Group 3 in Fig. 8) from the other soil samples analysed.

Fluvio-glacial materials of Late Pleistocene age were prevailing in the intermediate terrace T2 (630–660 m a.s.l.), also locally including some striated pebbles. These soils were poorly sorted, with a content of granular particles (46–54%) that was very close to the amount of silt and clay (54–46%). The composition of these materials was, on average: 30% gravel, 20% sand, 30% silt and 20% clay (Group 1 in Fig. 8). Based on their grain size distribution, these materials can be considered as sandy-clayey silts with a significant gravelly content. From the sedimentological viewpoint, the pelitic-sandy matrix can be considered as a loam.

The terraces pertaining to the highest elevations (T3–T5) are well differentiated from the lower ones for the widespread occurrence of

Table 3
Geotechnical index properties of the colluvial materials sampled from the detachment surfaces of the soil slips in the Chiarsò valley.

Sample	Depth	Wet unit weight γ	Dry unit weight γ_d	Specific gravity G_s	Void ratio e	Porosity n	Natural water content W	Saturated water content W_{sat}	Saturation degree S	Volumetric water content θ_w
	(m)	(kN/m^3)	(kN/m^3)	(–)	(–)	(%)	(%)	(%)	(%)	(m^3/m^3)
P45S1	1.5	21.87	17.95	2.71	0.51	34	18	19	95	0.33
P34S2	0.7	22.67	20.07	2.71	0.35	26	13	13	100	0.26
P36S2	0.5	18.50	13.46	–	–	–	37	–	–	–
P32S3	2.8	18.88	13.95	2.72	0.95	49	34	35	98	0.48
P33S2	1.3	19.69	15.26	2.68	0.76	43	29	29	100	0.43
P35S2	0.5	20.21	15.87	2.69	0.70	41	27	27	100	0.41
	mean	19.59	15.03	2.70	0.80	44	30	30	99	0.44
P16S1	1.3	17.70	14.03	–	–	–	26	–	–	–
P31S1	0.3	17.58	13.11	–	–	–	34	–	–	–
P30S2	0.5	18.70	13.62	2.71	0.99	50	36	37	99	0.49
P39S2	1.3	19.93	15.45	2.71	0.75	43	29	29	100	0.43
P43S3	1.0	18.38	14.18	2.72	0.92	48	30	34	88	0.42
P42S3	1.3	18.92	15.22	2.70	0.77	44	24	29	83	0.37
P05S2	0.4	19.11	15.35	2.69	0.76	43	24	28	86	0.38
P37S4	1.0	18.70	15.00	2.71	0.81	45	25	30	83	0.37
	mean	18.63	14.50	2.71	0.83	45	29	31	90	0.41
P26S4	0.5	17.90	13.47	2.78	1.06	52	27	38	71	0.36
P27S2	1.5	21.82	18.36	2.78	0.52	34	18	19	96	0.33
P38S2	1.2	–	–	2.69	0.60	37	22	22	100	0.37
	mean			2.75		41	22	26	89	0.35
P29S3	0.8	15.86	14.01	2.73	0.95	49	18	18	100	0.26
P28S3	0.6	16.07	13.97	2.75	0.97	49	18	18	100	0.25
P10S3	0.8	19.76	16.04	2.70	0.68	41	23	25	92	0.37
P13S4	0.6	20.48	16.93	2.75	0.62	38	21	21	100	0.35
	mean	18.04	15.24	2.73	0.80	44	20	21	98	0.31

Table 4
Shear strength properties of some colluvial samples collected from the soil slips in the Chiarsò valley.

Sample	Slide code	Depth	Peak shear strength		Residual shear strength	
		(m)	φ' (°)	c (kPa)	φ' (°)	c (kPa)
P26S4	P26	0.50	38.3	0.0	29.5	0.0
P27S2	P27	1.50	37.1	0.0	34.7	0.0
P32S1	P32	0.15	31.5	4.0	29.8	2.1
P32S3	P32	2.80	27.0	4.2	25.2	2.2
P32S4	P32	3.45	37.8	3.1	32.5	0.0
P35S2	P35	0.50	28.2	5.1	27.5	0.0
P43S3	P43	1.00	32.2	3.1	31.3	0.0

colluvial materials that derived from the alteration of the underlying parent bedrock. Terrace T3 (670–690 m a.s.l.) was characterised by the presence of a yellowish-brown colluvial cover. These sediments showed a prevailing silty fraction (34–53%), which was associated with not negligible fractions of clay (15–28%), sand (17–34%) and gravel (3–35%) (Group 2 in Fig. 8). The matrix mainly consists of sandy-clayey silt (as for slide P32) passing to clayey-sandy silt (slides P42 and P35).

The fluvio-glacial and colluvial terraces belonging to orders T2–T5 showed a typical three-layer stratigraphy, even if they were characterised by a variable thickness. Fig. 9 shows the stratigraphy of the colluvial deposit that was exposed at the crown scarp of slide P32, pertaining to order T3 (Table 2). Field observations pointed out the occurrence of eight distinct stratigraphic units that were grouped into three main soil layers (Fig. 9): (i) a 30 cm-thick surficial layer of an organic soil horizon with abundant root development (C1); (ii) a 270 cm-thick intermediate layer made up of a prevailing sand-silt-clay mixture (C2–C6); and (iii) a 50 cm-thick basal layer of a soil mixture that included cobbles and rock pieces (C7–C8).

When considering the USCS classification system, the analysed sediments can be classified on the basis of their grain size and plasticity properties as non-uniform soils with a mixed fine-coarse composition. The most frequent soils are the fine ones with medium to low plasticity (ML), along with the gravelly soils (GM) and the coarse soils with a considerable clayey loamy component (SM) (Fig. 8). The fine soils with medium plasticity (MH) are subordinate. All samples fell below the A-line in the Casagrande plasticity chart (Fig. 10a). The fine matrices of the sediments are substantially represented by inorganic clayey silts with low or medium plasticity and the colloidal activity of the clayey fraction is generally below the typical values of inactive soils (Fig. 10b). The valuesof the Atterberg limits and of the colloidal activity index (Fig. 10a, b) indicate that there is no correlation between the plasticity and activity characteristics of the materials and the specific type of slope instability.

The values of the liquid limit (LL) were compared with the water content at saturation (W_{sat}) of the samples to calculate the approximate mobility index (AMI), as formulated by Ellen and Fleming (1987) to express the predisposition of materials to fluidisation (Fig. 10c). Almost all samples fell within field B, which is defined by the condition $0.45 \leq AMI \leq 1$. This area of the graph corresponds with soils that may undergo partial fluidisation following an increase in water content. Only one sample fell within field C ($AMI \leq 0.45$), which includes soils that cannot incorporate enough water to fluidise and originate granular flows. The propensity of the sampled soils to fluidise upon failure was also evaluated by considering the liquidity index (LI), which has been used by previous authors to assess the fluidisation potential of soils upon failure (Locat and Demers, 1988; Kluger et al., 2022). According to the values determined in the laboratory, most of the samples were characterised by $LI \leq 0$, indicating a solid or semi-solid consistency. Only two samples, which are related to slides P32 and P33, had values of the liquidity index included in the range $0 \leq LI \leq 1.0$, corresponding to soils in a plastic state.

Table 3 shows some geotechnical properties of the sampled materials that include unit weight, specific gravity, void ratio, porosity and natural water content. The specific gravity of the solid fraction of the samples was generally constant, with an average value equal to 2.72; whereas the void ratio was variable, with values mainly included between $e = 0.5$ and $e = 1.0$ and an average value close to $e = 0.80$–0.85. The values of the natural water content (W) essentially vary in the range $W = 20$–30% (Table 3). The degree of saturation (S) is commonly high and equal to $S = 85$–90%, even if lower values were determined for slides P28 and P29 ($S = 50$–52%). These lower values of S are justified

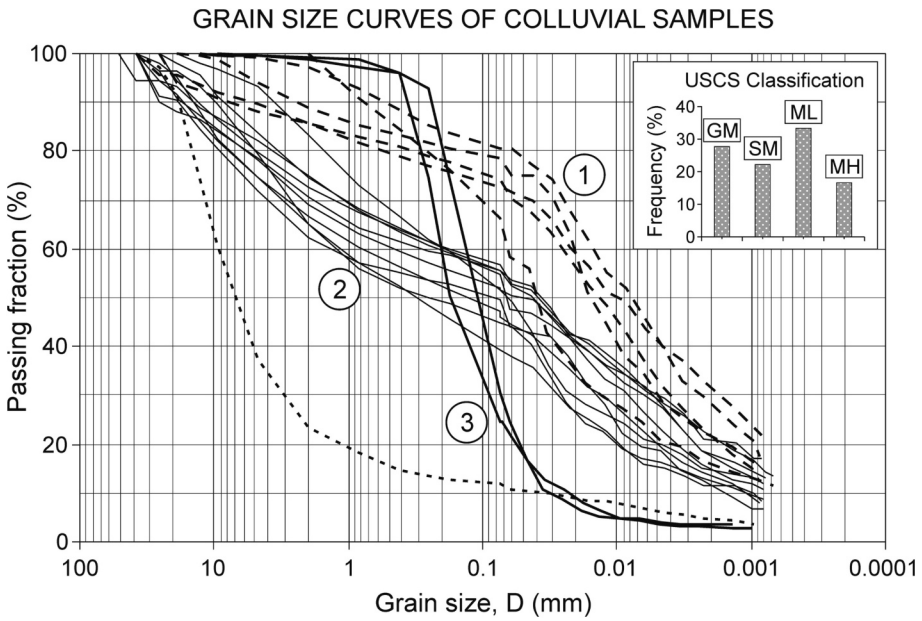

Fig. 8. Grain size distribution curves of the soils mobilised by the slide-debris flows of the Chiarsò valley. Note the three different groups of curves related to sets 1, 2 and 3.

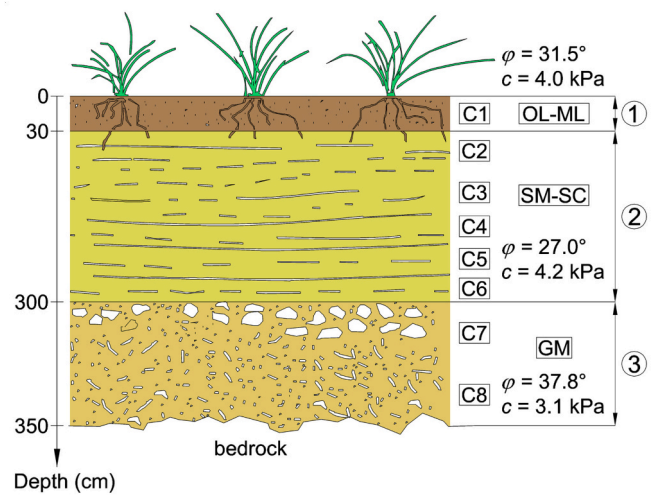

Fig. 9. Detailed stratigraphical section exposed at the crown scarp of slide P32. The USCS soil classification and peak shear strength properties of corresponding soil samples are also shown.

by the significant sandy content of the samples, which reflect a lower capacity of water retention of coarse soils. The volumetric water content (θ_w) has a quite constant value that is close to $\theta_w = 0.40$, ranging between 0.25 and 0.49. The high values of the natural water content obtained from the colluvial samples resulted in a low effective porosity (μ) of the soil (μ = 0.05–0.08), being μ the difference between the total porosity (n) and the volumetric water content. The effective porosity of the colluvial slopes in FVG is lower than the value (μ = 0.20) assumed in infiltration modelling of slopes in California (Pradel and Raad, 1993). This fact indicates that in the surficial soils of the alpine area of FVG the volume of the voids that can be filled by water during heavy rainfall is significantly lower, and consequently, the saturation condition can be reached in less time.

In order to evaluate possible seasonal variations of S of the colluvial deposits at depth, some soil moisture profiles were determined through measurements that were performed in both winter and summer. Measurements were carried out on soil samples that were collected from slide P32 (Paronuzzi et al., 2022), which occurred in T3 terrace order near Dioor (Fig. 5) and was characterised by the highest thickness value among all the slope failures analysed (Table 1).

Figure 11 shows two soil moisture profiles related to winter (Fig. 11a) and summer (Fig. 11b) periods, with variations of S at depth and the related trends of various mobile means (mm = 3, 6 and 8) (Fig. 11c, d). The general trend showed an increase in the degree of saturation as the depth increases, with values of S that wereclose to saturation starting from a depth of 200–250 cm. However, the moisture profiles were irregular, with saturation peaks that were separated by zones of lower water content (Fig. 11). At least three moisture peaks were recognisable: at depths of 30–60 cm, 130–170 cm, and 220 cm from the topographic surface. These peaks were found to be quite constant in the various seasons of the year. In addition, the minimum value of S was not related to the superficial soil horizon but was found at a greater depth (70–120 cm), without a significant seasonal variation. The soil moisture profiles also showed a remarkable constant average value of S of the colluvial deposit (about 85%).

Some suction measurements were also carried out using the pressure plate instrumentation (Meriggi, 1999), in order to reconstruct the Soil-water characteristic curve (SWCC) of the materials involved in slide P32 (Paronuzzi et al., 2022). In detail, the SWCC was determined by using the suction experimental measurements related to the intermediate colluvial layer and the equation proposed by Fredlund and Xing (1994), based on the parameters *a*, *n* and *m* (Fig. 12).

The shear strength properties of the colluvial materials were estimated in the laboratory by means of direct shear tests performed on seven samples that were collected from five selected slides. The soil sampling for the direct shear tests was performed at selected locations using steel samplers with an area of 60 × 60 mm and height of 20 mm, which are consistent with the size of the direct shear box. As for the slide P32, soil samples were collected from each of the three recognised layers (Fig. 9). The direct shear tests allowed us to determine both the peak and residual strengths of the tested materials.

The soil samples were placed in the direct shear apparatus and subsequently submerged in distilled water, thus the tests were performed in saturated conditions. Three different confining pressures were considered, namely 30 kPa, 54 kPa, and 79 kPa, which are consistent with stress values at the depths of sampling of the colluvial materials

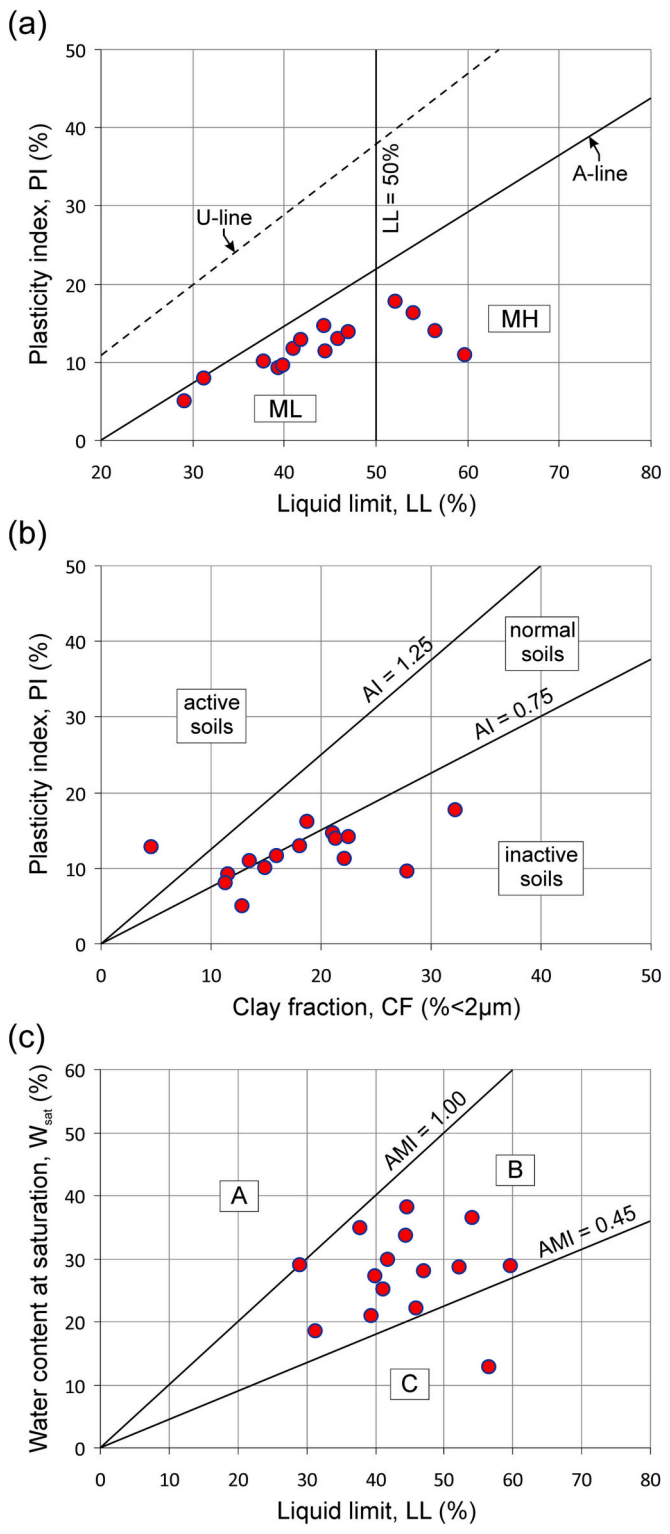

Fig. 10. (a) Plasticity chart, (b) activity chart, and (c) approximate mobility index (AMI) of the analysed colluvial samples ($n = 15$) involved in the shallow landslides in the Chiarsò valley.

(Fig. 13). The drained shear strength of the tested materials was assessed employing a very low displacement rate, equal to 0.015 mm/min, in order to avoid the development of pore-water overpressures. After reaching the peak shear strength for each sample, the shear stage was prolonged until stable residual strength conditions were reached at large deformations, which usually corresponds with centimetric displacements.

The results of the direct shear tests showed a slight difference between peak and residual strength values of the tested materials (Table 4 and Fig. 13). On the whole, values of the peak friction angle varied in the range 27–38°; whereas values of the residual friction angle were between 25 and 35°. As for the cohesion, peak values were in the range 0–5 kPa. The slight difference between peak and residual strength values as well as the null cohesion values at residual conditions reflect the scarce amount of clay fraction within the seven tested soil samples (CF = 11–28%). The aforementioned strength values are consistent with the shear resistance characteristics of poorly sorted silty sand soils (Salgado et al., 2000; Cho et al., 2006; Schnellmann et al., 2013).

4. Soil slip activation on terraced geometry

Some two-dimensional (2D) seepage and slope stability analyses were carried out to study shallow failures that can affect colluvial terraces in the mountain area of FVG. In detail, we firstly simulated the rainfall infiltration process occurring within a colluvial terrace as a result of some extreme hydrological events, and then we analysed slope stability according to the corresponding pore pressure variations. In this manner, we evaluated the stability of a terrace over time, investigating the critical conditions that are responsible for soil slip activation.

The infiltration process affecting the colluvial terrace was simulated by using the finite element method (FEM), in order to compute the suction and pore pressure variations along with the seepage vectors resulting from rainfall infiltration. The pore pressure distributions obtained from the transient seepage simulations were subsequently used as input data in the slope stability analyses, which were carried out employing the limit equilibrium method (LEM) in order to calculate the variations in the factor of safety (FoS) of the terrace. In the LEM analyses, the rigorous Morgenstern and Price (1965) method was adopted to calculate FoS. The 2D seepage and slope stability analyses were performed using the codes SEEP/W and SLOPE/W (Geo-Slope International Ltd., 2016), respectively.

The 2D calculation section of the terrace was set up on the basis of field evidence that was acquired from the shallow slope failures surveyed along the Chiarsò valley. The terrace is formed by a 20 m-long gently dipping tread (5°) and by a riser with an inclination equal to 40° and a length of about 15 m (Fig. 14). The terrace tread and riser were designed long enough to prevent possible influences of the boundary conditions on the pore pressure computation. The terrace tread is a 3-layer deposit whose stratigraphy was schematised as follows (Fig. 14):

1. a surficial 30 cm-thick soil layer;
2. a 120 cm-thick intermediate colluvial layer; and
3. a 150 cm-thick basal colluvial layer.

The porosity, the degree of saturation and suction values (h_0 and h_b) of the various soils, were assessed on the basis of the measurements carried out in the laboratory on soil samples (see section 3). However, despite the increasing curvilinear trend of the degree of saturation at depth that was ascertained on slide P32, the stratified deposit was schematised assuming different but constant values of the initial water content (θ_{S1}, θ_{S2} and θ_{S3}) and a corresponding degree of saturation (S_1, S_2 and S_3) for the various soil layers.

When considering the lack of specific in-situ infiltration measurements, the saturated permeability of the various soils was assumed on the basis of values reported in the literature (Tsaparas et al., 2002; Li et al., 2013; Rahardjo et al., 2013), with particular reference to the in-situ hydraulic conductivity (Lim et al., 1996; Dapporto et al., 2005; Jeong et al., 2017; Yang et al., 2017). In fact, the latter can be even 2–3 orders of magnitude greater than corresponding values obtained from laboratory tests on soil samples (Lim et al., 1996; Damiano et al., 2017). Particular attention has been paid to colluvial and/or residual materials, for which saturated permeability values varying in the range $k = 1 \times$

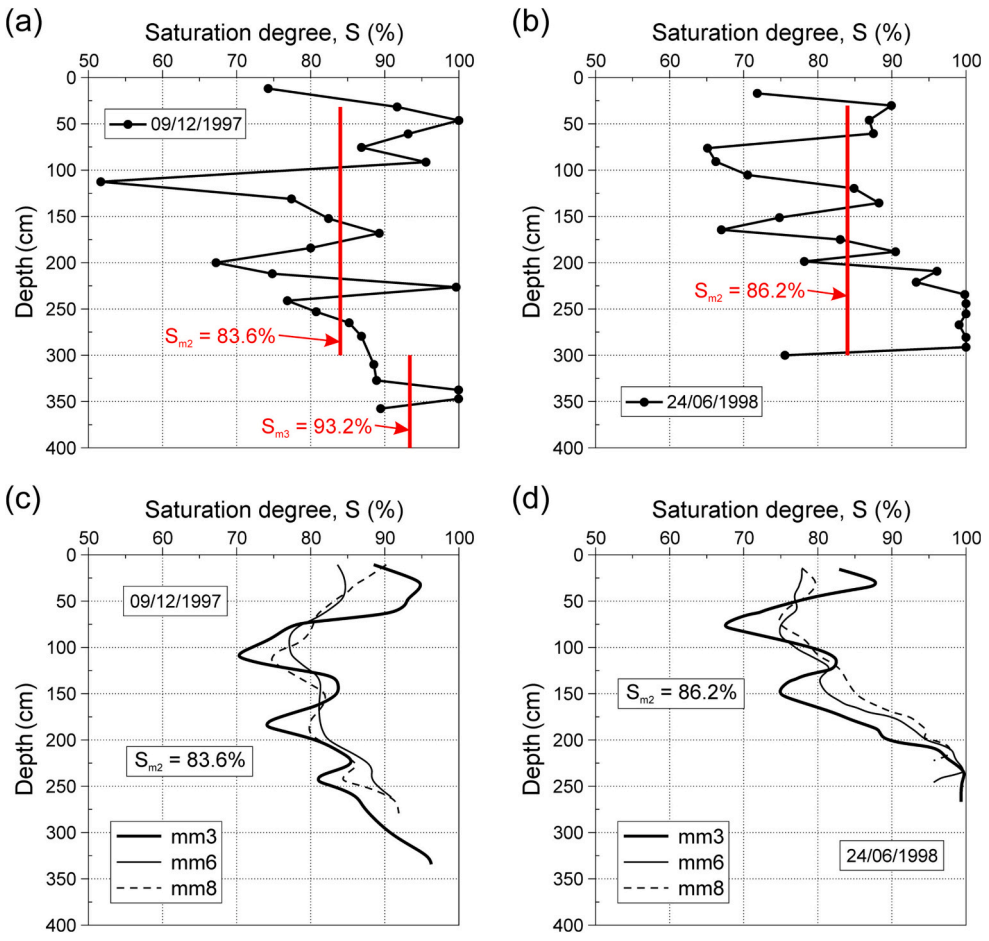

Fig. 11. Variations of the degree of saturation within the terraced slope at Dioor (slide P32) measured in (a) winter and (b) summer, and (c)–(d) the related trends of various mobile means (mm = 3, 6 and 8).

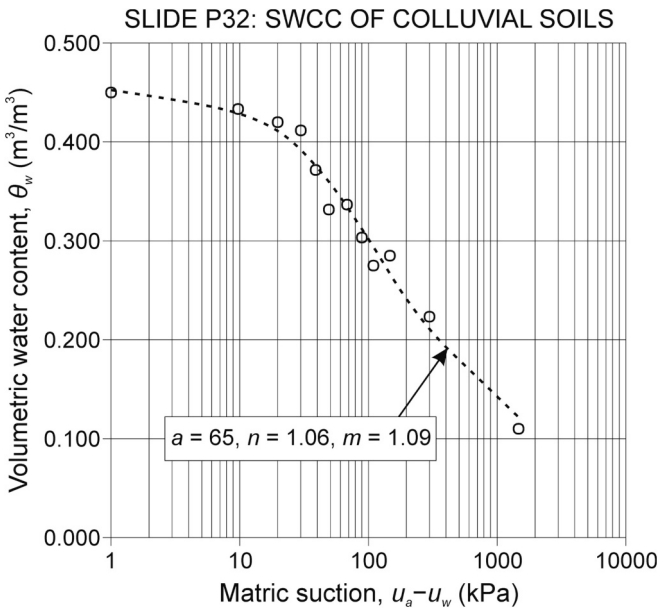

Fig. 12. Soil–water characteristic curve related to the Dioor colluvial deposit (modified from Paronuzzi et al., 2022).

10^{-4}–1×10^{-6} m/s were suggested (Ng and Shi, 1998; Dai et al., 1999; Gasmo et al., 2000; Rahimi et al., 2011; Cuomo and Della Sala, 2013; Balzano et al., 2019).

Therefore, the following values were assumed as representative for the saturated permeability at the slope scale of the three soil layers forming the terrace tread, decreasing from the top to the bottom: (i) $k_1 = 10^{-4}$ m/s for the high-permeable surficial organic soil; (ii) $k_2 = 10^{-5}$ m/s for the sandy-silty-clayey intermediate colluvium; and (iii) $k_3 = 10^{-6}$ m/s for the silty-clayey basal layer. These values are only indicative and describe the average behaviour of the various materials, thus being useful to verify the influence of hydrological stratifications within the colluvial cover on the rainfall infiltration process.

In order to take into account possible variations in the permeability of the unsaturated soil during the infiltration process, different volumetric water content and hydraulic conductivity functions were assigned to the hydrogeological units, depending on the matric suction and according to their saturated permeability. The hydraulic permeability functions were evaluated according to the soil-water characteristic curve reconstructed on the basis of the suction experimental measurements previously presented (Fig. 12). The terrace riser is made up of a soil layer of a variable thickness (0.3–0.7 m), with the same characteristics as the soil horizon at the top of the terrace tread (Fig. 14). In addition, a fourth material was considered, which corresponds to a saturated bedrock of very low permeability ($k_4 = 10^{-8}$ m/s).

As for the mechanical properties, the involved soils were modelled as Mohr-Coulomb materials, and the values of unit weight, cohesion and friction angle were assumed according to the results of the geotechnical laboratory tests (Table 4). Notably, when assessing shear strength

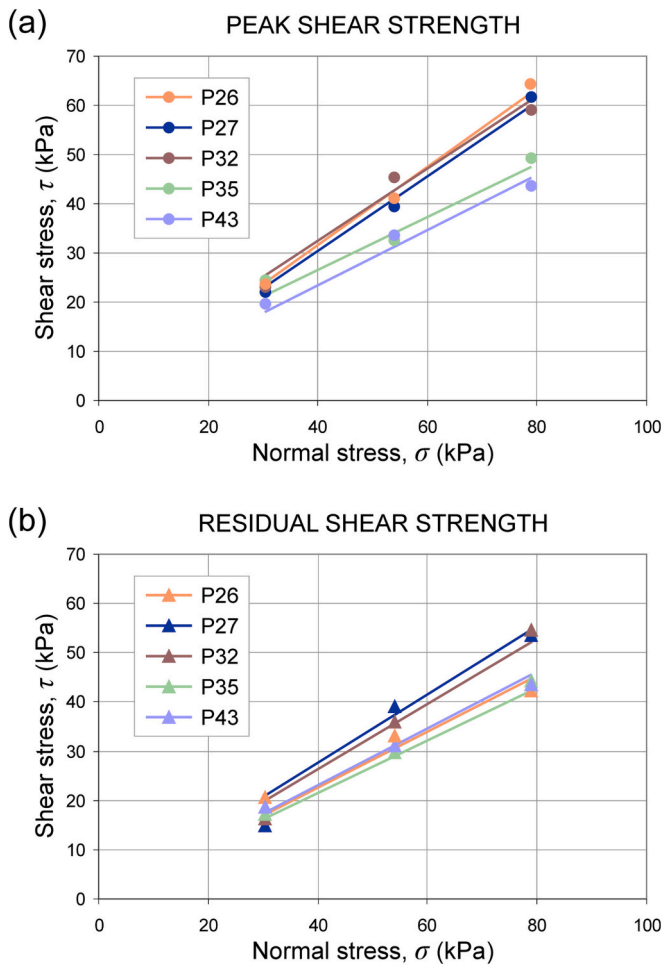

Fig. 13. Failure envelopes and experimental values of shear strength of the soil samples tested in the direct shear apparatus for (a) peak and (b) residual conditions.

properties of colluvial soils in slope stability analyses, the following issues have to be considered:

1. The extremely heterogeneous nature of the colluvial materials makes sampling difficult, and a certain degree of disturbance is unavoidable. In particular, at a low depth and for low confining pressures, the sampling of soil mixtures including coarser elements can result in a compaction of the soil, which in turn, causes an increase in the soil shear strength (Wästerlund, 2020);
2. A very important factor affecting the measured soil parameters is the size of the sample tested in the direct shear apparatus (scale effect) (Stefanow and Dudziński, 2021). In particular, some studies have found that the measured internal friction angle in sands and clayey sands decreased as the size of the measurement box increased (Cerato and Lutenegger, 2006; Wu et al., 2008; Dadakh et al., 2010). This scale effect in the box can be explained by the smaller ratio of the sample length to the median grain diameter (L/D_{50}) if compared with the actual size of the shear zone in correspondence with the slope failure surface (Wu et al., 2008; Zhou et al., 2009); and
3. In slope stability analyses adopting the LEM, one basic assumption is that the peak shear strength is attained simultaneously along the entire rupture surface. Many soils that include a significant fine fraction, like loamy soils that make up colluvial covers, demonstrate strain-softening behaviour. For these soils, it is unreasonable to assume that the soil reaches its peak strength simultaneously at all points along the failure surface (Wu, 1996). If the soil had previously experienced large deformations at some points on the rupture surface, particularly along the terrace risers that may have been involved in previous sliding processes (see section 2.2), the strength at these points is reduced to residual strength.

Based on the aforementioned issues, in-situ shear strength properties of colluvial soils can be lower than strength values estimated on laboratory samples. Consistently, the values of the friction angle and cohesion of the materials modelled in the slope stability analyses were assumed as included between peak and residual values. Therefore, the mechanical parameters of the three soil layers were as follows: (i) $\gamma_1 = 17.0$ kN/m^3, $\varphi_1 = 30.0°$, $c_1 = 3.8$ kPa; (ii) $\gamma_2 = 18.9$ kN/m^3, $\varphi_2 = 25.5°$, $c_2 = 2.2$ kPa; and (iii) $\gamma_3 = 19.6$ kN/m^3, $\varphi_3 = 33.5°$, $c_3 = 2.0$ kPa. The bedrock was considered as an impenetrable material. In addition, the unit weight in the unsaturated zone and the matric suction of the modelled materials were computed from each corresponding volumetric water content function.

The finite element mesh was set up as regularly as possible, only employing quadrilateral elements with an average size of 0.1 m × 0.1 m (46,283 nodes and 45,831 elements), which are much more suitable for modelling ground surface processes because the primary unknown gradients are usually steeper in a direction perpendicular to the surface (Geo-Slope International Ltd., 2016). In the 0.3 m-thick soil horizon at the top of the terrace tread, the mesh was designed to be denser (seven elements in the Y-direction) in order to properly simulate the infiltration process within this layer.

Particular attention was paid to both boundary and initial conditions. A drainage condition was set up at the upslope extremity of the terrace tread as well as at the lower end of the terrace riser (Fig. 14). The drainage condition allowed for simulating the seepage process and the water discharge properly, avoiding the onset of excessive and unrealistic pore-water pressures. Differently, a permeability threshold (no flux boundary condition) was assumed at the base of the model to prevent undesired water outflow. Rainfall was applied at the surface mesh boundary (i.e., on the topographic surface) as a water unit flux (m/s) vs. time (s) function. Furthermore, water was not allowed to pond on the surface mesh boundary, and the "potential seepage face review" option was set up to guarantee that computed pressures at the mesh nodes on the topographic surface were not greater than zero, as positive pressure on the surface indicates ponding, which cannot happen along the sloping boundary.

The initial conditions of the seepage modelling were set up in two well-defined stages. In the first stage, a steady-state simulation was carried out to initialise the hydrogeological properties of the modelled materials on the basis of their volumetric water content and hydraulic conductivity functions. The second stage was performed in order to obtain an initial degree of saturation for each of the three soil layers that was consistent with the measurements actually acquired in the field. To this aim, we carried out a preliminary transient analysis in which a design hyetograph made up of an alternation of dry and rainfall periods was iteratively determined until reaching the desired values of water content of the three soil layers.

Then, when performing the transient seepage analyses to study the effects of an extreme hydrological event, two different rainfall patterns were considered (Fig. 14). In the first case, an idealised hyetograph was assumed, which considers a 5-h rainfall with a variable intensity of 30–40–60–40–30 mm/h (Case 1). This idealised rainfall pattern has a cumulated height of 200 mm over 5 h, which corresponds to a reference extreme hydrological event that occurs in the mountain area of FVG with a return period of about 150–200 years (Paronuzzi et al., 1998). In the second case, we assumed the key span of precipitation that actually fell in the Chiarsò valley on 22 June 1996 (Fig. 4), which coincided with a 5-h rainfall with an intensity of 90–30–55–30–23 mm/h and was responsible for all the soil slips that occurred in the valley (Case 2a). In addition, in order to test the influence of the initial saturation degree of the soils on the stability condition of the colluvial terrace, we also

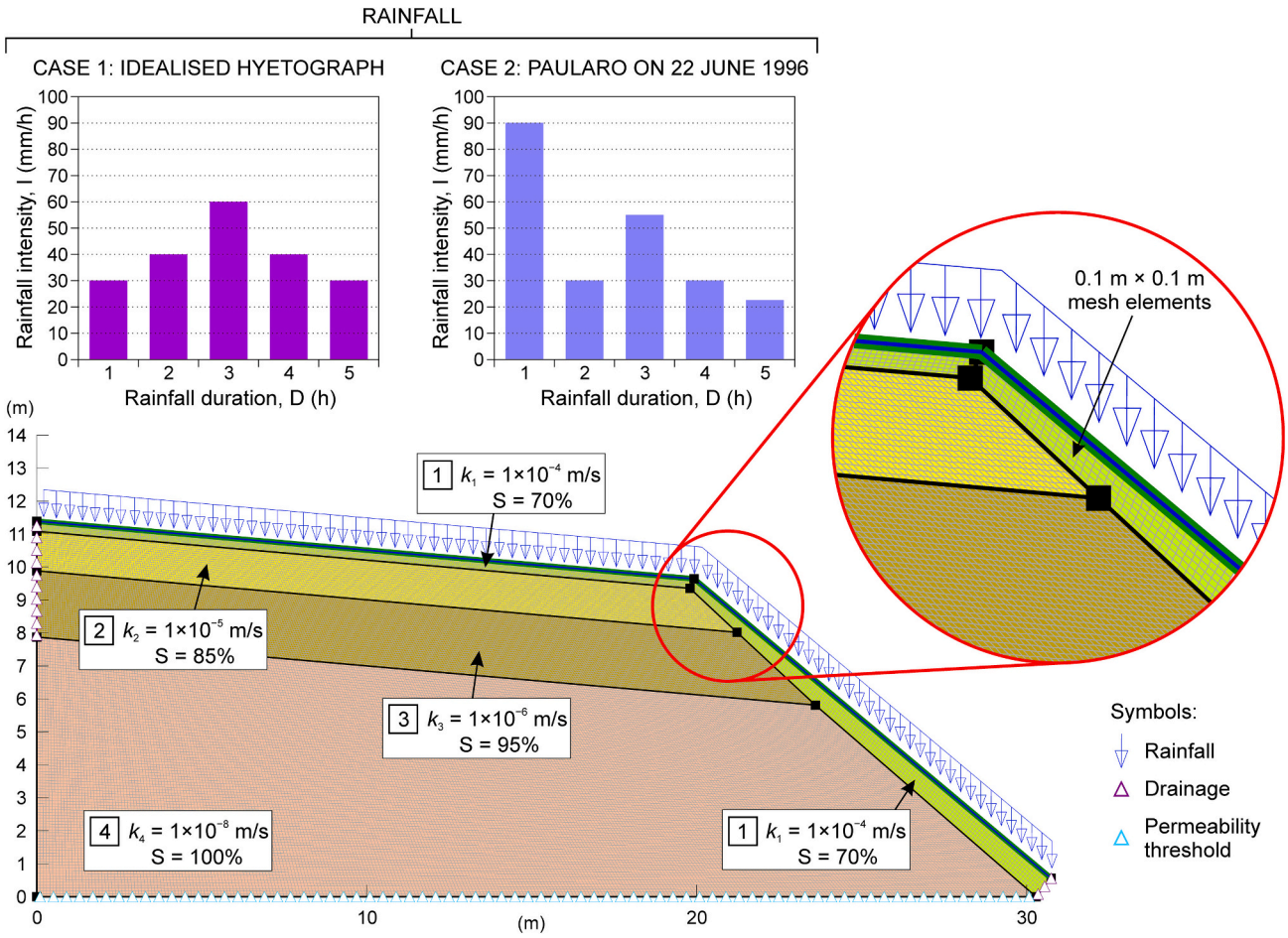

Fig. 14. Calculation section of the simulated colluvial terrace showing the mesh, the saturated permeability and the degree of saturation of the soil layers, along with the boundary condition applied to the seepage modelling. Two different rainfall patterns were considered in the models: an idealised hyetograph and the precipitation actually fell on 21–22 June 1996.

carried out a simulation based on the rainfall pattern on 22 June 1996 that was directly computed after the initial steady-state simulation, i.e., without performing the preliminary transient analysis (Case 2b). In all the three cases analysed, the transient seepage simulations were prolonged up to fourteen days after the rainfall end, in order to fully appreciate the progressive desaturation of the terrace and the related changes in slope stability.

The results of the transient seepage simulation related to Case 2a are shown in Fig. 15, in which the computed variations of the volumetric water content, the seepage vectors and the location of the ground water table are drawn at some specific steps over the analysis, starting from the initial saturation condition before the occurrence of the simulated rainfall event (Fig. 15a). After the first hour of heavy rainfall, characterised by an intensity of 90 mm/h (Fig. 15b), the infiltration process results in the onset of an ephemeral water table within the saturated soil layer on the terrace riser. This water table is sustained by the permeability threshold represented by the basal contact with the underlying bedrock and is associated with a downward sub-parallel seepage. On the terrace tread, a top-down saturation front forms within the intermediate colluvial layer. In addition, at the rim of the terrace, a riser-to-tread water inflow occurs, favouring a rapid saturation of the outer part of the colluvial deposit that is behind the surficial soil layer (Fig. 15b). After three hours of rainfall (cumulated intensity of 90–30–55 mm/h), the terrace is affected by two advancing saturation fronts (Fig. 15c). A top-down front moving towards the basal colluvial layer and a riser-to-tread front that advances laterally inside the terrace. The combined action of these two advancing fronts causes the rapid saturation of the intermediate colluvial layer and a related pore pressure increase. In addition, a bottom-up saturation starts from the layer 1-layer 2 interface within the top soil horizon (Fig. 15c). The terrace riser is also characterised by significant downward seepage vectors.

At the end of the simulated rainfall event (Fig. 15d), the soil layer at the top of the tread is near-fully saturated owing to the advancement of the bottom-up front that reaches the topographic surface. As a result, a seepage process initiates within the top soil layer and towards the terrace riser, which also causes an increase in pore pressures in the outermost part of the terrace. The seepage vectors are sub-parallel to the layer 1-layer 2 interface (that is, with a dip of 5°), but at the terrace rim the ground water table lowers due to the increasing velocities related to the inclination change between the tread and the riser. Simultaneously, the two deeper saturation fronts advance both downward and inside the terrace, causing a progressive saturation of the basal colluvial layer (Fig. 15d).

Three hours after the precipitation ends (Fig. 15e), the more permeable surface soil layer is subjected to a rapid desaturation due to the water discharge along the riser, which also causes a lowering of the ground water table and a temporary decrease in the pore pressure. In the outer part of the colluvial terrace, this rapid desaturation causes the separation of the two saturation fronts, but the internal one continues to move downward, progressively saturating the basal colluvial layer. Six hours after the rainfall ends (Fig. 15f), the saturation front reaches the layer 3-bedrock interface, determining the full saturation of the terrace tread, which in turn, causes a rise in the ground water table and a related pore pressure increase. As a result, in the outer part of the terrace, a

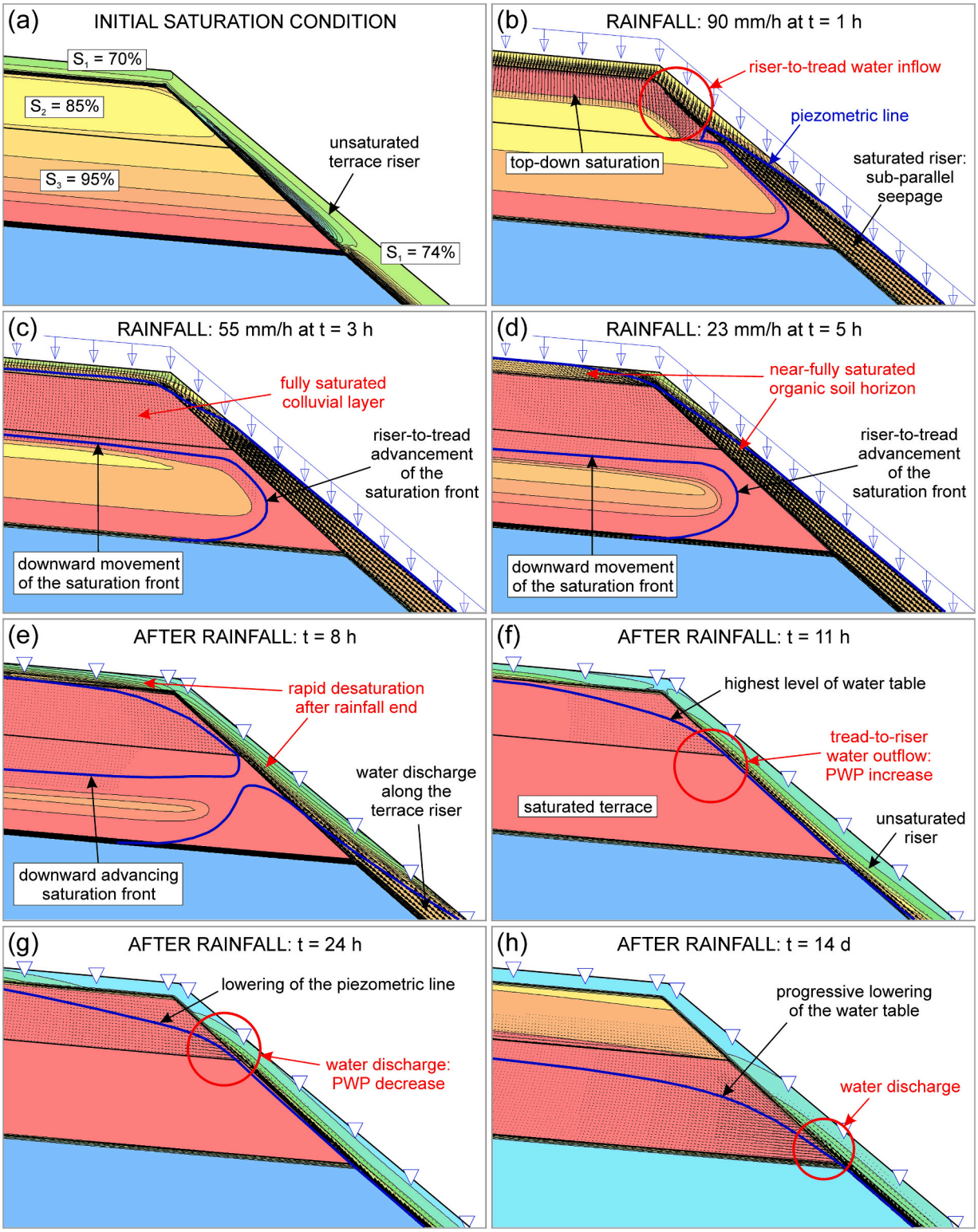

Fig. 15. Variations of the volumetric water content and piezometric line at some paramount stages (a)–(h) of the simulated infiltration process within a colluvial terrace, which were calculated assuming the rainfall which fell on 21–22 June 1996 and the actual initial saturation degree of the involved soil layers. The seepage vectors are also shown.

tread-to-riser water outflow is triggered. This water outflow is favoured by the unsaturated riser and is fed by the saturated tread, which acts as a supplying reservoir. From this moment on, the water discharge along the riser causes a slow but progressive desaturation of the terrace and a consequent lowering in the ground water table (Fig. 15g). After two weeks (Fig. 15h), the intermediate colluvial layer is unsaturated, whereas the basal colluvium is still partially saturated owing to its lower permeability, which is responsible for the delayed water discharge.

The slope stability analysis allowed us to estimate the factor of safety of the colluvial terrace over time, i.e., before, during and after the

occurrence of an extreme hydrological event. It must also be noted here that the main aim of this analysis is that of evaluating the FoS variations rather than to calculate the exact FoS values at some paramount moments, which are strictly dependent on the assumed shear strength properties that are, in turn, difficult to define at the slope scale. This means that, the most important contribution of the performed slope stability analysis is that of identifying the most critical moments in the stability condition that the colluvial terrace experiences as a result of an extreme rainfall event.

The initial stability condition of the colluvial terrace (Fig. 16a), which was calculated before rainfall commences on the basis of suction values of the unsaturated soils, is quite far from the critical condition (FoS = 1.60). This value of FoS is associated with a slip surface that is mainly located at the base of the top soil layer on the terrace riser. As a result of heavy rainfall and the related increase in pore pressures, the terraced slope reaches a first failure condition (FoS = 0.94) at the end of the simulated precipitation (Fig. 16b). Notably, slope failure only involves the soil layer along the terrace riser, where pore pressures are higher during the initial stages of rainfall infiltration. This failure condition is consistent with the actual soil slip activation that, according to eyewitnesses, occurred during the peaks of intense precipitation. In these circumstances, slope failure can occur at various distances from the tread rim, thus explaining the variable distance between the slide crown and the terrace border that was ascertained from field observations. Notably, the failure surface has a quite planar geometry and was formed in correspondence with or slightly above the contact with the underlying bedrock.

The terraced slope reaches a second failure condition (FoS = 0.98) six hours after the rainfall ends (Fig. 16c), that is when the terrace tread is fully saturated and is characterised by the highest values of pore pressure due to a tread-to-riser water outflow (see Fig. 15f). In these circumstances, slope failure involves the outermost part of the terrace tread, along a circular slip surface whose upslope end is located behind the terrace rim. This slope failure type is consistent with most soil slips that were activated in correspondence with the tread border, and which are related to hydrogeological conditions that commonly occur some hours after the rainfall ends.

When considering the variations of FoS over time (Fig. 16d), the value of FoS rapidly decreases during the rainfall event owing to the annulment of suction in the soil and the subsequent increase in pore pressures. However, among the three cases simulated, Case 1 shows a slower decrease of FoS that is caused by a lower rainfall intensity within the first two hours of precipitation (30 mm/h and 40 mm/h of the idealised hyetograph) and the consequent lower amount of water that infiltrates within the soil. Differently, Case 2a shows a sharper decrease in the value of FoS that depends on both the higher initial degree of saturation of the soils and the higher intensity of the first hour of precipitation (90 mm/h), which caused a more rapid saturation of the soil layer of the terrace raiser. As a result, the failure condition (FoS < 1.00) is achieved slightly before than the other cases (Fig. 16d). The lowest values of FoS, which were calculated at the end of rainfall, determine a reduction in slope stability of about 40% compared with the initial stability condition. After reaching the first negative peak of FoS, the subsequent rapid desaturation of the more permeable soil layer at top of the scarp determines an increase of about 15% in the value of FoS (Fig. 16d).

Then, FoS decreases due to the full-saturation of the terrace tread, up to reaching a second negative peak. Interestingly, only Case 2a leads to slope failure; whereas in Case 1 and Case 2b FoS is almost equal and higher than 1.00 (Fig. 16d). This fact emphasises the key influence of the initial saturation condition of the soil layers in the rainfall infiltration process and pore pressure distribution within the terrace. In particular,

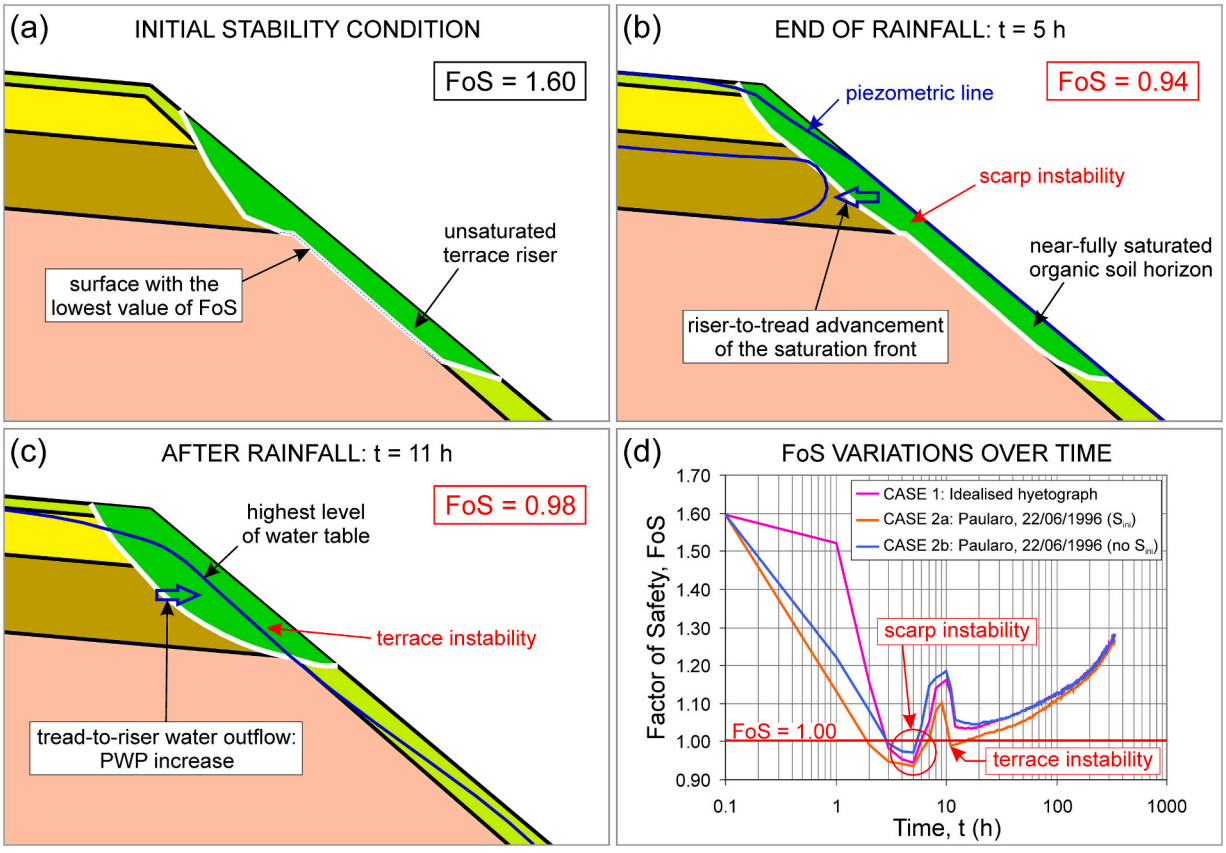

Fig. 16. Critical slip surface and associated value of FoS of the analysed terraced slope at: (a) initial condition before heavy rainfall commences; (b) end of heavy rainfall (90–30–55–30–23 mm/h); and (c) six hours after the rainfall ends. (d) Variations of FoS over time for the three cases simulated (note the logarithmic x-axis).

an underestimation of the initial degree of saturation may lead to a dangerous overestimation of the actual slope stability condition. Finally, the progressive lowering in the piezometric line caused by the water discharge along the riser results in a gradual increase in the slope stability of the terrace, which gains a recovery of FoS of about 20% after two weeks (Fig. 16d).

5. Discussion and conclusions

Fluvial terraces originated from fill-and-cut sedimentary processes that followed the deglaciation of the alpine valleys have already been described in the literature related to various mountain regions in the Alps, in particular in large basins or in correspondence with the major stream confluences (Surian, 1996; Surian and Pellegrini, 2000; Colucci et al., 2014). The characteristic geomorphological configuration of the alpine terraces is related to the occurrence of the near-flat tread and the moderately steep riser. From an engineering geological perspective, alpine terraces characterised by thin (0.5–3.0 m) stratified covers of colluvial materials are often involved in shallow failures (soil slips) when the area is hit by very intense rainfall, even of a limited duration. The shallow landslides related to the Chiarsò valley case history confirm the vulnerability of these types of slopes when they are affected by extreme hydrological events. Notably, research on shallow landslides involving alpine terraces related to deglaciation is lacking in the literature. As a result, this paper represents the first attempt to investigate the hydrological conditions and mechanisms that are responsible for the activation of soil slips on alpine colluvial terraces subject to rainstorms.

The typical stratigraphy of colluvial terraces occurring in the mountain area of FVG is characterised by a 3-layer deposit with diminishing saturated permeability (Paronuzzi et al., 2022). The presence of variably sorted soils with a high content of fine fraction (50% of silt and clay) and an associated medium-to-low permeability ($k = 10^{-5}$–10^{-6} m/s) represents a predisposing geological factor for slope instability of terraced landforms subject to intense precipitation. In addition, the rainfall infiltration numerical modelling performed within this study emphasised the strong influence of abrupt variations in the permeability of the various soil layers forming the terraced slope on the infiltration process at depth. Indeed, the inner hydrogeological discontinuities determine, particularly in the case of highly intense precipitation ($I \geq 60$ mm/h), the formation of a perched water table that moves simultaneously upwards and downwards, particularly starting from the organic soil-colluvium interface. During the infiltration process, localised pore-water overpressures can rise at the main hydrological discontinuities within the colluvial deposit, as also proved by field monitoring of groundwater flows in unsaturated soil slopes (Zhang et al., 2000; Leung and Ng, 2013; Zhang et al., 2019). Therefore, one another unfavourable predisposing factor for slope stability is represented by the occurrence of significant variations in the hydraulic conductivity that are induced by the stratification of the colluvial deposit or by the presence of an underlying bedrock at low depth.

The most critical areas affected by slide-debris flows are the tops of the terrace risers, that is just below the edges of the terrace treads, as ascertained by extensive field observations performed along the Chiarsò valley after the rainstorm on 21–22 June 1996 and also reported by previous authors for other Alpine slopes (Moser and Hohensinn, 1983). This evidence demonstrates that the top of the terrace riser is characterised by the most unfavourable hydrogeological condition for the slope stability. Outcomes of the 2D seepage and slope stability analyses demonstrated that the soil slip activation can occur at two different stages during the infiltration process and are driven by different failure mechanisms. The first critical stability condition is reached during the phases of greater precipitation intensity or at the end of a rainstorm, whereas the second critical condition is achieved some hours after the rainfall ends. Both phenomena determine a considerable reduction in the factor of safety of the slope, which can achieve failure even in the case of a high initial stability condition, i.e., before heavy rainfall commences ($FoS > 1.5$).

Modelling results showed that, during the extreme hydrological event, the rainfall infiltration within the soil voids rapidly saturates the soil layer on the terrace riser and causes the onset of an ephemeral subsurface water table that is sustained by the permeability threshold represented by the basal contact with the underlying bedrock and is associated with a seepage sub-parallel to the slope face. This finding is consistent with previous investigations on the seepage process within saturated slope debris covers overlying an inclined bedrock at a low depth (Dapporto et al., 2005; Baum et al., 2010; Yang et al., 2017; Balzano et al., 2019). As a result of saturation, the resistance contribution due to suction is lost and positive pore-water pressures rise, causing a rapid decrease in the shear strength of the material and possibly bringing the terrace scarp into a critical stability condition and causing its eventual failure. The quick process of saturation is consistent with the numerous testimonies that describe the activation of shallow landslides during the phases of maximum intensity of the precipitation (Brand et al., 1984; Paronuzzi et al., 1998; Dai et al., 1999).

Concurrently, the thicker and less permeable terrace tread is subjected to an infiltration process that is mainly influenced by possible localised decreases in the downward hydraulic conductivity, which cause a progressive but slower saturation of the colluvial deposit, despite the presence of a highly permeable top organic soil. This means that the whole saturation of the terrace tread can occur some hours after the rainfall ends, when the desaturation of the more permeable terrace riser has already commenced. At the tread edge, the change in the inclination of the slope profile determines the onset of a tread-to-riser water outflow. The main source of water supply for the outward seepage is represented by the gently dipping terrace treads, which stored a large amount of water during the peak rainfall stages (reservoir-like effect). These outflows are controlled in a decisive manner by the geometry of the bedrock and by the trend of the main hydrological discontinuities. This hydrological-driven effect is mainly related to the organic soil-colluvium and layer 2-layer 3 interfaces, which are characterised by abrupt variations in the permeability caused by the silty-clayey materials of the colluvial deposit. This process determines a rapid increase in the pore-water pressure in the outer part of the colluvial terrace, causing a second critical moment of slope stability condition and potentially leading to failure, even some hours after the rainfall ends.

The achievement of the failure condition of a colluvial terrace is strictly related to the initial degree of saturation of the materials involved. In fact, the progressive saturation process is accompanied by a simultaneous, rapid decrease in the soil suction (Lim et al., 1996; Urcioli et al., 2016; Wang et al., 2020). The value of this negative capillary pressure substantially depends on the degree of saturation of the soil and on the grain size characteristics of the material (Rahardjo et al., 2019; Wang et al., 2022; Wu et al., 2022). If the soil layer is close to saturation, as typically occurs in the wettest periods characterised by frequent precipitations, the value of suction is low or close to zero, as highlighted by experimental measurements within this study. In these circumstances, the volumetric water content necessary to bring the soil to saturation is very low. When the soil permeability is close to or lower than the rainfall intensity, the soil layer that can be saturated is thicker. Otherwise, the saturation of the surficial soil layer cannot be reached. The latter occurs for highly permeable soils, in which the infiltration rate is higher than the intensity of the precipitation falling on the topographical surface. The performed seepage and slope stability analyses stressed the importance of a proper evaluation of the initial degree of saturation of the soil layers forming the stratified terrace, which can be obtained through adequate experimental measurements at different depths within the colluvial deposit (Paronuzzi et al., 2022). In particular, an underestimation of S can lead to a dangerous overestimation of the stability condition of the slope during the occurrence of the extreme hydrological event.

The shallow slope failures described can be classified as slide-debris

flows, whose failure process initiates as a planar or slightly circular sliding but can evolve in a single or multiple debris flow. The possible activation of a debris flow is related to the achievement of the critical state corresponding with the fluidisation of the mobilised material (Iverson et al., 1997; Haq et al., 2023). The debris flow is the result of an undrained deformation of the soil that occurs in the presence of a typically contractive behaviour (Sassa and Wang, 2005; Iverson and George, 2014). Due to the continuous deformation in the basal shear zone, very small load increases are sufficient to overcome the peak resistance. Under these conditions, the material reaches an undrained residual strength (soil softening) and small load increases are enough to cause mass mobilisation of the debris cover.

Finally, this study has showed that a critical value of rainfall intensity of about 40–45 mm/h was responsible for the saturation of the alpine colluvial terraces and the activation of soil slips in the mountain basins of FVG. Notably, this critical value has been determined on the basis of an engineering geological characterisation of specific rainfall-induced shallow landslides and differs methodologically from threshold values only obtained through statistic-based landslide susceptibility analyses related to regional-scale hydrological studies (e.g., Wei et al., 2018). This value of rainfall intensity should be considered as a rainfall threshold for similar mountain basins characterised by a humid continental climate and by the occurrence of colluvial deposits with a high content of fine fraction originated by weathering of terrigenous rock mass sequences.

Author statement

Alberto Bolla on behalf of the authors states that all authors have seen and approved the final version of the manuscript being submitted. We warrant that the article is the authors' original work, hasn't received prior publication and isn't under consideration for publication elsewhere.

Funding

This research received no specific grant from any funding agency in the public, commercial, or not-for-profit sectors.

Authors' contribution

Authors make substantial contributions to conception and design, and/or acquisition of data, and/or analysis and interpretation of data.

Declaration of Competing Interest

The authors declare that they have no known competing financial interests or personal relationships that could have appeared to influence the work reported in this paper.

Data availability

Data will be made available on request.

References

Balzano, B., Tarantino, A., Ridley, A., 2019. Preliminary analysis on the impacts of the rhizosphere on occurrence of rainfall-induced shallow landslides. Landslides 16, 1885–1901.
Baum, R.L., Godt, J.W., Savage, W.Z., 2010. Estimating the timing and location of shallow rainfall-induced landslides using a model for transient, unsaturated infiltration. J. Geophys. Res. 115, F03013.
Beck, H.E., Zimmermann, N.E., McVicar, T.R., Vergopolan, N., Berg, A., Wood, E.F., 2018. Present and future Köppen-Geiger climate classification maps at 1-km resolution. Sci. Data 5, 180214.
Bellugi, D.G., Milledge, D.G., Cuffey, K.M., Dietrich, W.E., Larsen, L.G., 2021. Controls on the size distributions of shallow landslides. Proc. Natl. Acad. Sci. U. S. A. 118, e2021855118.
Brand, E.W., Premchitt, J., Phillipson, H.B., 1984. Relationship between rainfall and landslides in Honk Hong. In: Proc. 4th Int. Symp. Landslides, Toronto, pp. 377–384.
Camera, C.A.S., Apuani, T., Masetti, M., 2014. Mechanisms of failure on terraced slopes: the Valtellina case (northern Italy). Landslides 11, 43–54.
Campbell, R.H., 1974. Debris flows originating from soil slips during rainstorms in southern California. Q. J. Eng. Geol. 7, 339–349.
Campbell, R.H., 1975. Soil Slips, Debris Flows, and Rainstorms in the Santa Monica Mountains and Vicinity, Southern California. Professional Paper 851,. U.S. Geological Survey, Washington, D.C.
Cancelli, A., Nova, R., 1985. Landslides in soil debris cover triggered by rainstorms in Valtellina (Central Alps, Italy). In: Sassa, K. (Ed.), Proceedings 4th Int. Conference and Field Workshop on Landslides. The Japanese Landslide Soc, Tokyo, Japan, pp. 267–272.
Cerato, A.B., Lutenegger, A.J., 2006. Specimen size and scale effects of direct shear box tests of sands. Geotech. Test. J. 29, 507–516.
Cevasco, A., Pepe, G., Brandolini, P., 2014. The influences of geological and land use settings on shallow landslides triggered by an intense rainfall event in a coastal terraced environment. Bull. Eng. Geol. Environ. 73, 859–875.
Cho, G.-C., Dodds, J., Santamarina, J.C., 2006. Particle shape effects on packing density, stiffness, and strength: natural and crushed sands. J. Geotech. Geoenviron. Eng. 132, 591–602.
Cho, S.E., 2009. Infiltration analysis to evaluate the surficial stability of two-layered slopes considering rainfall characteristics. Eng. Geol. 105, 32–43.
Cho, S.E., 2017. Prediction of shallow landslide by surficial stability analysis considering rainfall infiltration. Eng. Geol. 231, 126–138.
Colucci, R.R., Monegato, G., Žebre, M., 2014. Glacial and proglacial deposits of the Resia Valley (NE Italy): new insights on the onset and decay of the last Alpine Glacial Maximum in the Julian Alps. Alpine Mediterran. Quatern. 27, 85–104.
Crosta, G.B., 1990. A study of slope movements caused by heavy rainfall in Valtellina (Italy, July 1987). In: Cancelli, A. (Ed.), ALPS 90, 6th Int. Conf. and Field Workshop on Landslides, September 1990, Milan (Italy). Univ. Milano Spec. Pubbl, Milan, Italy, pp. 247–258.
Crosta, G.B., 1994. Rainfall thresholds applied to soil slips in alpine and prealpine areas. In: Proc. 1st Int. Symp. Protection and Development of the Environment in the Mountains Area, June 20–24 1994, Ponte di Legno, Italy, pp. 141–153.
Crosta, G.B., Dal Negro, P., 2003. Observations and modelling of soil slip-debris flow initiation processes in pyroclastic deposits: the Sarno 1998 event. Nat. Hazards Earth Syst. Sci. 3, 53–69.
Crosta, G.B., Frattini, P., 2003. Distributed modelling of shallow landslides triggered by intense rainfall. Nat. Hazards Earth Syst. Sci. 3, 81–93.
Crosta, G.B., Dal Negro, P., Frattini, P., 2003. Soil slips and debris flows on terraced slopes. Nat. Hazards Earth Syst. Sci. 3, 31–42.
Cruden, D.M., Varnes, D.J., 1996. Landslides types and processes. In: Turner, A.K., Schuster, R.L. (Eds.), Special Report 247: Landslides: Investigation and Mitigation. TRB, National Research Council, Washington, pp. 36–75.
Cuomo, S., Della Sala, M., 2013. Rainfall-induced infiltration, runoff and failure in steep unsaturated shallow soil deposits. Eng. Geol. 162, 118–127.
Dadakh, R., Ghafoori, M., Ajalloeian, R., Lashkaripour, G.R., 2010. The effect of scale direct shear tests on the strength parameters of clayey sand in Isfahan city, Iran. J. Appl. Sci. 18, 2027–2033.
Dai, F.C., Lee, C.F., Wang, S., 1999. Analysis of rainstorm-induced slide-debris flows on natural terrain of Lantau Island, Hong Kong. Eng. Geol. 51, 279–290.
D'Amato Avanzi, G., Giannecchini, R., Puccinelli, A., 2004. The influence of the geological and geomorphological settings on shallow landslides. An example in a temperate climate environment: the June 19, 1996 event in Northwest Tuscany (Italy). Eng. Geol. 73, 215–228.
D'Amato Avanzi, G., Falaschi, F., Giannecchini, R., Puccinelli, A., 2009. Soil slip susceptibility assessment using mechanical-hydrological approach and GIS techniques: an application in the Apuan Alps (Italy). Nat. Hazards 50, 591–603.
Damiano, E., Greco, R., Guida, A., Olivares, L., Picarelli, L., 2017. Investigation on rainwater infiltration into layered shallow covers in pyroclastic soils and its effect on slope stability. Eng. Geol. 220, 208–218.
Dapporto, S., Aleotti, P., Casagli, N., Polloni, G., 2005. Analysis of shallow failures triggered by the 14-16 November 2022 event in the Albaredo valley, Valtellina (Northern Italy). Adv. Geosci. 2, 305–308.
Di Crescenzo, G., Santo, A., 2005. Debris slides-rapid earth flows in the carbonate massifs of the Campania region (Southern Italy): morphological and morphometric data for evaluating triggering susceptibility. Geomorphology 66, 255–276.
Ellen, S.D., Fleming, R.W., 1987. Mobilization of debris flows from soil slips, San Francisco Bay region, California. In: Costa, J.E., Wieczorek, G.F. (Eds.), Reviews in Engineering Geology, vol. VII, Debris flows/avalanches: Process, Recognition and Mitigation, 7. Geological Society of America, Boulder, Colorado, pp. 31–40.
Fan, C.C., Su, C.F., 2008. Role of roots in the shear strength of root-reinforced soils with high moisture content. Ecol. Eng. 33, 157–166.
Fredlund, D.G., Xing, A., 1994. Equations for the soil-water characteristic curve. Can. Geotech. J. 31, 521–532.
Froude, M.J., Petley, D.N., 2018. Global fatal landslide occurrence from 2004 to 2016. Nat. Hazards Earth Syst. Sci. 18, 2161–2181.
Gariano, S.L., Guzzetti, F., 2016. Landslides in a changing climate. Earth Sci. Rev. 162, 227–252.
Gasmo, J.M., Rahardjo, H., Leong, E.C., 2000. Infiltration effects on stability of a residual soil slope. Comput. Geotech. 26, 145–165.
Gatto, M.P.A., Montrasio, L., 2023. X-SLIP: a SLIP-based multi-approach algorithm to predict the spatial-temporal triggering of rainfall-induced shallow landslides over large areas. Comput. Geotech. 15, 105175.

Geo-Slope International Ltd., 2016. Seepage and Stability Modeling with SEEP/W and SLOPE/W. Users Manuals. (Calgary, Alberta, Canada).
Giannecchini, R., 2006. Relationship between rainfall and shallow landslides in the southern Apuan Alps (Italy). Nat. Hazards Earth Syst. Sci. 6, 357–364.
Godt, J.W., Baum, R.L., Lu, N., 2009. Landsliding in partially saturated materials. Geophys. Res. Lett. 36, L02403.
Graber, A., Santi, P., Meza Arestegui, P., 2021. Constraining the critical groundwater conditions for initiation of large, irrigation-induced landslides, Siguas River Valley, Peru. Landslides 18, 3753–3767.
Guzzetti, F., Cardinali, M., Reichenbach, P., Cipolla, F., Sebastiani, C., Galli, M., Salvati, P., 2004. Landslides triggered by the 23 November 2000 rainfall event in the Imperia Province, Western Liguria, Italy. Eng. Geol. 73, 229–245.
Guzzetti, F., Peruccacci, S., Rossi, M., Stark, C.P., 2007. Rainfall thresholds for the initiation of landslides in central and southern Europe. Meteorog. Atmos. Phys. 98, 239–267.
Guzzetti, F., Peruccacci, S., Rossi, M., Stark, C.P., 2008. The rainfall intensity-duration control of shallow landslides and debris flows: an update. Landslides 5, 3–17.
Haq, S., Indraratna, B., Nguyen, T.T., Rujikiatkamjorn, C., 2023. Hydromechanical state of soil fluidisation: a microscale perspective. Acta Geotech. 18, 1149–1167.
Haque, U., da Silva, P.F., Devoli, G., Pilz, G., Zhao, B., Khaloua, A., Wilipo, W., Andersen, P., Lu, P., Lee, J., Yamamoto, T., Keellings, D., Wu, J.-H., Glass, G.E., 2019. The human cost of global warming: deadly landslides and their triggers (1995-2014). Sci. Total Environ. 682, 673–684.
Hou, X., Vanapalli, S.K., Li, T., 2018. Water infiltration characteristics in loess associated with irrigation activities and its influence on the slope stability in *Heifangtai* loess highland, China. Eng. Geol. 234, 27–37.
Hungr, O., McDougall, S., Wise, M., Cullen, M., 2008. Magnitude–frequency relationships of debris flows and debris avalanches in relation to slope relief. Geomorphology 96, 355–365.
Hungr, O., Leroueil, S., Picarelli, L., 2014. The Varnes classification of landslide types, an update. Landslides 11, 167–194.
Iverson, R.M., George, D.L., 2014. A depth-averaged debris-flow model that includes the effects of evolving dilatancy. I. Physical basis. Proc. R. Soc. A 470, 20130819.
Iverson, R.M., Reid, M.E., LaHusen, R.G., 1997. Debris-flow mobilization from landslides. Annu. Rev. Earth Planet. Sci. 25, 85–138.
Ivy-Ochs, S., Monegato, G., Reitner, J.M., 2023. The Alps: Glacial landforms during the deglaciation (18.9–14.6 ka). In: Palacios, D., Hughes, P.D., García-Ruiz, J.M., Andrés, N. (Eds.), European Glacial Landscapes, the Last Deglaciation. Elsevier, pp. 175–183.
Jeong, S., Lee, K., Kim, J., Kim, Y., 2017. Analysis of rainfall-induced landslide on unsaturated soil slopes. Sustainability 9, 1280.
Johnson, K.A., Sitar, N., 1990. Hydrologic conditions leading to debris flow initiation. Can. Geotech. J. 27 (6), 789–801.
Kesseli, J.E., 1943. Disintegrating soil slips of the coast ranges of Central California. J. Geol. 51 (5), 342–352.
Kluger, M.O., Jorat, M.E., Moon, V.G., Kreiter, S., de Lange, W.P., Mörz, T., Robertson, T., Lowe, D.J., 2020. Rainfall threshold for initiating effective stress decrease and failure in weathered tephra slopes. Landslides 17, 267–281.
Kluger, M.O., Kreiter, S., Moon, V.G., Roskoden, R.R., Mörz, T., 2022. Compressibility and permeability of weathered, sensitive volcanic ash (tephra) deposits at the Omokoroa flow slide, New Zealand. Eng. Geol. 310, 106885.
Leung, A.K., Ng, C.W.W., 2013. Seasonal movement and groundwater flow mechanism in an unsaturated saprolitic hillslope. Landslide 10, 455–467.
Li, W.C., Lee, L.M., Cai, H., Li, H.L., Dai, F.C., Wang, M.L., 2013. Combined roles of saturated permeability and rainfall characteristics on surficial failure of homogeneous soil slope. Eng. Geol. 153, 105–113.
Li, X., Lizárraga, J.J., Buscarnera, G., 2021. Regional-scale simulation of flowslide triggering in stratified deposits. Eng. Geol. 292, 106248.
Lim, T.T., Rahardjo, H., Chang, M.F., Fredlund, D.G., 1996. Effects of rainfall on matric suctions in a residual soil slope. Can. Geotech. J. 33, 618–628.
Locat, J., Demers, D., 1988. Viscosity, yield stress, remolded strength, and liquidity index relationships for sensitive clays. Can. Geotech. J. 25, 799–806.
Meriggi, R., 1999. Misura delle proprietà idrauliche e meccaniche dei terreni colluviali in condizione di parziale saturazione. In: Proceedings of the XX Convegno Nazionale di Geotecnica, AGI, Parma 22–25 settembre 1999, pp. 177–184.
Montrasio, L., 2000. Stability analysis of soil-slip. In: Brebbia, C.A. (Ed.), Risk Analysis II. Wit press, Southampton, UK, pp. 357–366.
Montrasio, L., Valentino, R., Losi, G.L., 2011. Towards a ral-time susceptibility assessment of rainfall-induced shallow landslides on a regional scale. Nat. Hazards Earth Syst. Sci. 11, 1927–1947.
Morgenstern, N.R., Price, V.E., 1965. The analysis of the stability of general slip surfaces. Géotechnique 15, 79–93.
Moser, M., Hohensinn, F., 1983. Geotechnical aspects of soil slips in alpine regions. Eng. Geol. 19, 185–211.
Ng, C.W.W., Shi, Q., 1998. A numerical investigation of the stability of unsaturated soil slopes subjected to transient seepage. Comput. Geotech. 22 (1), 1–28.
Okada, Y., Ochiai, H., Okamoto, T., Sassa, K., Fukuoka, H., Igwe, O., 2007. A complex eart slide-earth flow induction by the heavy rainfall in July 2006, Okaya City, Nagano Prefecture, Japan. Landslides 4, 197–203.
Paronuzzi, P., Vanon, R., 1995. Eventi pluviometrici critici e dissesti: studio della franosità del Comune di Paularo (Friuli – Alpi Carniche). Geoingegn. Ambient. Minera. 85, 21–31.
Paronuzzi, P., Coccolo, A., Garlatti, G., 1998. Eventi meteorici critici e debris flows nei bacini montani del Friuli. L'Acqua. Riv. It. Idrol. Tecn. 6, 39–50.
Paronuzzi, P., Del Fabbro, M., Bolla, A., 2022. Soil moisture profiles of unsaturated colluvial slopes susceptible to rainfall-induced landslides. Geosciences 12, 12010006.
Peng, D., Xu, Q., Liu, F., He, Y., Zhang, S., Qi, X., Zhao, K., Zhang, X., 2018. Distribution and failure modes of the landslides in Heitai terrace, China. Eng. Geol. 236, 97–110.
Pike, R.J., Sobieszczyk, S., 2008. Soil slip/debris flow localized by site attributes and wind-driven rain in the San Francisco Bay region storm of January 1982. Geomorphology 94, 290–313.
Pradel, D., Raad, G., 1993. Effect of permeability on surficial stability of homogenous slopes. J. Geotechn. Eng. ASCE 119 (2), 315–332.
Querini, R., 1984. Il nubifragio delle Alpi Carniche Orientali (11 settembre 1983) ed i conseguenti dissesti idrogeologici. Ann. Academ. Ital. Sci. Forest. 23, 3–52.
Rahardjo, H., Ong, T.H., Rezaur, R.B., Leong, E.C., Fredlund, D.G., 2010. Response parameters for characterization of infiltration. Environ. Earth Sci. 60, 1369–1380.
Rahardjo, H., Satyanaga, A., Leong, E.-C., 2013. Effects of flux boundary conditions on pre-water pressure distribution in slope. Eng. Geol. 165, 133–142.
Rahardjo, H., Kim, Y., Satyanaga, A., 2019. Role of unsaturated soil mechanics in geotechnical engineering. Intern. J. Geo-Eng. 10, 8.
Rahimi, A., Rahardjo, H., Leong, E.-C., 2011. Effect of antecedent rainfall patterns on rainfall-induced slope failure. J. Geotech. Geoenviron. Eng. 137, 483–491.
Ray, R.L., Jacobs, J.M., de Alba, P., 2010. Impacts of unsaturated zone soil moisture and groundwater table on slope stability. J. Geotech. Geoenviron. Eng. 136, 1448–1458.
Rice, R.M., Corbett, E.S., Bailey, R.G., 1969. Soil slips related to vegetation, topography, and soil in Southern California. Water Resour. Res. 5, 647–659.
Salciarini, D., Fanelli, G., Tamagnini, C., 2017. A probabilistic model for rainfall-induced shallow landslide prediction at the regional scale. Landslides 14, 1731–1746.
Salgado, R., Bandini, P., Karim, A., 2000. Shear strength and stiffness of silty sand. J. Geotech. Geoenviron. Eng. 126, 451–462.
Sassa, K., Wang, G.-H., 2005. Mechanism of landslide-triggered debris flows: Liquefaction phenomena due to the undrained loading of torrent deposits. In: Jakob, M., Hungr, O. (Eds.), Debris-Flow Hazards and Related Phenomena. Springer, Chichester, UK, pp. 81–104.
Schilirò, L., Cevasco, A., Esposito, C., Scarascia Mugnozza, G., 2018. Shallow landslide initiation on terraced slopes: inferences from a physically based approach. Geomat. Nat. Hazar. Risk 9, 295–324.
Schnellmann, R., Rahardjo, H., Schneider, H.R., 2013. Unsaturated shear strength of a silty sand. Eng. Geol. 162, 88–96.
Segoni, S., Piciullo, L., Gariano, S.R., 2018. A review of the recent literature on rainfall thresholds for landslide occurrence. Landslides 15, 1483–1501.
Seguinot, J., Ivy-Ochs, S., Jouvet, G., Huss, M., Funk, M., Preusser, F., 2018. Modelling last glacial cycle ice dynamics in the Alps. Cryosphere 12, 3265–3285.
Shakoor, A., Smithmyer, A.J., 2005. An analysis of storm-induced landsides in colluvial soils overlying mudrock sequences, southestern Ohio, USA. Eng. Geol. 78, 257–274.
Sidle, R.C., Pearce, A.J., O'Loughlin, C.L., 1985. Hillslope Stability and Land Use. Water Resources Monograph 11. American Geophysical Union, Washington, D.C., p. 140
Stark, C.P., Hovius, N., 2001. The characterization of landslide size distributions. Geophys. Res. Lett. 28, 1091–1094.
Stefanow, D., Dudziński, P.A., 2021. Soil shear strength determination methods – State of the art. Soil Tillage Res. 208, 104881.
Sun, P., Wang, H., Wang, G., Li, R., Zhang, Z., Huo, X., 2021. Field model experiments and numerical analysis of rainfall-induced shallow loess landslides. Eng. Geol. 295, 106411.
Surian, N., 1996. The terraces of the Piave River in the Vallone Bellunese (Eastern Alps, Italy). Geogr. Fis. Din. Quat. 19, 119–127.
Surian, N., Pellegrini, G.B., 2000. Paraglacial sedimentation in the Piave Valley (Eastern Alps, Italy): an example of fluvial processes conditioned by glaciation. Geogr. Fis. Dinam. Quat. 23, 87–92.
Tsaparas, I., Rahardjo, H., Toll, D.G., Leong, E.C., 2002. Controlling parameters for rainfall-induced landslides. Comput. Geotech. 29, 1–27.
Urcioli, G., Pirone, M., Comegna, L., Picarelli, L., 2016. Long-term investigations on the pore pressure regime in saturated and unsaturated sloping soils. Eng. Geol. 212, 98–119.
Varnes, D.J., 1978. Slope Movement Types and Processes. In: Schuster, R.L., Krizek, R.J. (Eds.), Special Report 176: Landslides: Analysis and Control. TRB, National Research Council, Washington, pp. 11–33.
Venturini, C., 2001. Carta geologica delle Alpi Carniche—Scala 1:25,000 (Selca, Florence, 2 maps).
Wakatsuki, T., Matsukura, Y., 2008. Lithological effects in soil formation and soil slips on weathering-limited slopes underlain by granitic bedrocks in Japan. Catena 72, 153–168.
Wang, F., Dai, Z., Takahashi, I., Tanida, Y., 2020. Soil moisture response to water infiltration in a 1-D slope soil column model. Eng. Geol. 267, 105482.
Wang, Y., Li, T., Hou, X., Zhang, Y., Li, P., 2022. Hydraulic modeling of water flow in the thick vadose zone under precipitation. Geoenviron. Disast. 9, 7.
Wästerlund, I., 2020. Soil and Root Damage in Forestry. Reducing the Impacts of Forest Mechanization. Elsevier, p. 187.
Wei, L.-W., Huang, C.-M., Chen, H., Lee, C.-T., Chi, C.-C., Chiu, C.-L., 2018. Adopting the I_3–R_{24} rainfall index and landslide susceptibility for the establishment of an early warning model for rainfall-induced shallow landslides. Nat. Hazards Earth Syst. Sci. 18, 1717–1733.
Wen, B.P., Aydin, A., 2005. Mechanism of a rainfall-induced slide-debris flow: Constraints from microstructure of its slip zone. Eng. Geol. 78, 69–88.
Wu, D., Liu, H., Wang, C., Xu, X., Liu, X., Wang, Q., 2022. The interaction effect of particle composition and matric suction on the shear strength parameters of unsaturated granite residual soil. Arab. J. Sci. Eng. 47, 12453–12467.

Wu, P.-K., Matsushima, K., Tatsuoka, F., 2008. Effects of specimen size and some other factors on the strength and deformation of granular soil in direct shear tests. Geotech. Test. J. 31, 45–64.
Wu, T.H., 1996. Soil strength properties and their measurement. In: Landslides: Investigation and Mitigation. In: Special Report 247, Transportation Research Board. National Academy of Sciences, pp. 319–336.
Yang, K.-H., Uzuoka, R., Thuo, J.N., Lin, G.-L., Nakai, Y., 2017. Coupled hydro-mechanical analysis of two unstable unsaturated slopes subject to rainfall infiltration. Eng. Geol. 216, 13–30.
Zhang, C.-B., Chen, L.-H., Liu, Y.-P., Ji, X.-D., Liu, X.-P., 2010. Triaxial compression test of soil-root composites to evaluate influence of roots on soil shear strength. Ecol. Eng. 36, 19–26.
Zhang, J., Jiao, J.J., Yang, J., 2000. In situ rainfall infiltration studies at a hillside in Hubei Province, China. Eng. Geol. 57, 31–38.
Zhang, M., Yin, Y., Hu, R., Wu, S., Zhang, Y., 2011. Ring shear test for transform mechanism of a slide-debris-flow. Eng. Geol. 118, 55–62.
Zhang, M., Yang, L., Ren, X., Zhang, C., Zhang, T., Zhang, J., Shi, X., 2019. Field model experiments to determine mechanisms of rainstorm-induced shallow landslides in the Feiyunjiang River basin, China. Eng. Geol. 262, 105348.
Zhou, Q., Shen, H.H., Helenbrook, B.T., Zhang, H., 2009. Scale dependence of direct shear tests. Chin. Sci. Bull. 54, 4337–4348.